Mucosal Immunology 18 (2025) 1405–1423

Contents lists available at ScienceDirect

Mucosal Immunology

journal homepage: www.elsevier.com/mi

Article

Epididymitis promotes formation of tertiary lymphoid organs in the cauda epididymidis

Hiba Hasan [a,b], Christiane Pleuger [a,b], Dingding Ai [a,b], Sudhanshu Bhushan [a,b], Eva Wahle [a,b], Tara Procida-Kowalski [c], Qunxiong Zeng [d], Rukmali Wijayarathna [e,f], Claire Xin Sun [g], Yong-Gang Duan [d], Daniela Fietz [b,h], Marek Bartkuhn [c], Hans-Christian Schuppe [b,i], Adrian Pilatz [b,i], Kate L. Loveland [e,f], Andreas Meinhardt [a,b,e], Mark P. Hedger [e,f], Monika Fijak [a,b,*]

[a] Institute of Anatomy and Cell Biology, Justus Liebig University of Giessen, Giessen, Germany
[b] Hessian Centre of Reproductive Medicine, Justus Liebig University of Giessen, Giessen, Germany
[c] Biomedical Informatics and Systems Medicine Science Unit for Basic and Clinical Medicine, Justus Liebig University of Giessen, Giessen, Germany
[d] Shenzhen Key Laboratory of Fertility Regulation, The University of Hong Kong - Shenzhen Hospital, Shenzhen, China
[e] Centre for Reproductive Health, Hudson Institute of Medical Research, Clayton, VIC Australia
[f] Department of Molecular and Translational Sciences, Monash University, Clayton, VIC Australia
[g] Centre for Cancer Research, Hudson Institute of Medical Research, Clayton, VIC Australia
[h] Department of Veterinary Anatomy, Histology and Embryology, Justus Liebig University of Giessen, Germany
[i] Department of Urology, Paediatric Urology and Andrology, Justus Liebig University of Giessen, Germany

ARTICLE INFO

Keywords:
Tertiary lymphoid organ
High endothelial venules
Epididymis
Uropathogenic *Escherichia* coli
Epididymitis
Male infertility

ABSTRACT

Uropathogenic *Escherichia coli* is a common pathogen that affects the cauda epididymidis, causing interstitial edema, epithelial damage, leukocyte infiltration, and fibrosis. Despite antibiotic treatment, up to 20 % of patients develop abscesses in the cauda epididymidis, and 40 % experience low sperm counts. To understand the mechanisms of infertility impairment caused by epididymitis, we aimed to investigate the histopathological and immunological changes affecting the cauda epididymidis focusing on later post-acute stages of UPEC infection. Using a bacterial mouse model of acute epididymitis, we identified organized tertiary lymphoid organs (TLOs) that formed in the cauda epididymidis at 28 days post-infection. These appear as compartmentalized B- and T-cell clusters containing high endothelial venules (HEV) with evidence of an active germinal centre. Transcriptomic analysis confirmed the existence of a supportive microenvironment conducive to TLO formation and maintenance. Furthermore, TLO formation was also observed in human cauda epididymidis following chronic epididymitis, as documented by the presence of B- and T-cell clusters adjacent to HEV. Elevated concentrations of CXCL13 were measured in sera from epididymitis patients in acute and post-acute phase of disease. Our data suggest that TLOs in the cauda epididymidis harbor a functionally active germinal centre, which may impact male fertility in the long term.

Introduction

Uropathogenic *Escherichia coli* (UPEC) is the major bacterial pathogen leading to urinary tract infections, including acute epididymitis when spreading to the male genital tract.[1] Male patients with a UPEC infection usually present with unilateral scrotal pain and swelling. Despite adequate antibiotic treatment, approximately 20 % of the patients exhibit epididymal abscesses, which can be detected via ultrasound or palpation in the cauda, and ~40 % experience long-term impaired fertility.[2–3] The underlying pathological changes have been pinpointed to the cauda epididymidis, where interstitial edema, loss of epithelial integrity, leukocyte infiltration within the ducts and the interstitial space, and fibrosis have been reported.[1,4–5] Such alterations can impair sperm maturation and secretory functions of the epididymis, leading to duct obstruction with subsequent oligospermia or azoospermia.[4–5]

* Corresponding author at: Institute of Anatomy and Cell Biology, Justus Liebig University of Giessen, Aulweg 123, D-35392 Giessen, Germany.
E-mail address: monika.fijak@anatomie.med.uni-giessen.de (M. Fijak).

https://doi.org/10.1016/j.mucimm.2025.10.001
Received 10 February 2025; Accepted 5 October 2025
Available online 10 October 2025
1933-0219/© 2025 The Author(s). Published by Elsevier Inc. on behalf of Society for Mucosal Immunology. This is an open access article under the CC BY license (http://creativecommons.org/licenses/by/4.0/).

The epididymis is a highly convoluted duct that is divided into the caput, corpus, and cauda regions in men and an additional initial segment in mouse.[5–6] As spermatozoa transit through the epididymis, they interact with secretions from the epididymal epithelium and undergo biochemical and physiological modifications. These changes enable them to acquire progressive motility and undergo hyperactivation to potentiate their fertilizing ability. By the time reaching the cauda, spermatozoa have attained nearly all of the structural and functional attributes required for successful fertilization.[7–8] The epididymis displays distinct regional characteristics that reflect the complexity of its functions. These differences are largely due to the variability in the molecular and cellular landscape along its length.[9–11] Among the key contributors to this heterogeneity are immune cells, which play a crucial role in maintaining the epididymal integrity.[12–13] Immune cell populations, particularly mononuclear phagocytes, vary along the length of the epididymis, illustrating a shift from immune tolerance in the proximal regions to immune defense in the distal regions. In mice, the proximal epididymis is dominated by $CX3CR1^{+}$ macrophages with homeostatic profiles, while other immune cell populations account for <5 % of leukocytes. In contrast, the distal epididymis contains higher proportions of monocyte-derived cells and dendritic cells. This region is also enriched with lymphocytes exhibiting innate immunity like-properties, such as natural killer and γδ T-cells, as well as pro-inflammatory monocyte-derived $CCR2^{+}MHCII^{+}$ cells.[5,9,13–14]

Inflammation is an essential mechanism to restore tissue homeostasis after injury or infection. If unresolved, persistent inflammation can lead to failed immunoregulation that culminates in the formation of organized immune cell infiltrates known as tertiary lymphoid organs (TLOs), which develop ectopically and postnatally in non-lymphoid organs.[15–16] TLOs likely provide an immune niche to support adaptive immunity, much like secondary lymphoid organs (SLOs) such as the spleen, Peyer's patches, and lymph nodes. Unlike SLOs, TLOs are not developmentally controlled and can form anywhere in the body.[17] Inflammation-driven TLO development has been described in almost every organ, with their organization, maturation status, and complexity depending on the inflammatory stimulus and host tissue.[15,18–20] Their formation and function in the body, however, is largely enigmatic.

TLOs originate as loosely organized B- and T-cell clusters that are initially mixed, but can acquire regional segregation into distinct B- and T-cell areas as seen in SLOs.[16] To support anatomical and cellular composition similar to that of SLOs, TLOs rely on the expression of hemostatic lymphoid chemokines (including CXCL13, CCL21, and CCL19) and the presence of high endothelial venules (HEVs).[16,19,21] HEVs are specialized blood vessels that deliver naïve and memory lymphocytes from the bloodstream to lymphoid organs, thus helping regulate immune responses.[22–23]

TLO formation near organs that harbor cells with highly immunogenic antigens can exacerbate immune dysregulation.[19–20,24] The testis and epididymis are prime examples, as they harbor germ cells at various stages of development that are highly immunogenic.[4] While injury, infection and inflammation in these organs are potentially curable, male reproductive function can still be impacted.[25–26] Indeed, TLO elements in the testis have been described, with HEVs implicated in recruiting cytotoxic T lymphocytes in testicular seminoma[27] and follicular-like structures comprising distinct B- and T-cell clusters containing dendritic cells were found in testicular germ cell tumors.[28–29] Recently, the presence of TLO components was reported in the epididymis of mice depleted of regulatory T-cells.[30]

Deeper understanding of the inflammatory-induced damage and immunopathologies specifically targeting the cauda epididymidis, following UPEC infection is warranted, given the fact that, despite adequate antibiotic treatment, a large percentage of patients suffer from persistent fertility disturbances.[2–3,9] This prompted us to examine and analyze the longitudinal histopathological changes and immunological alterations affecting the cauda epididymidis in pre-clinical models of acute bacterial infection and inflammation using UPEC as a relevant pathogen and chronic autoimmune epididymitis for the potential formation of TLOs.

Materials and methods

Animals

Adult (10–12 week old) C57BL6/J mice were purchased from Charles River Laboratories (Sulzfeld, Germany) and the Monash University Animal Research Platform. Animals were maintained in specific pathogen-free conditions (12 h light/dark cycle, 20–22 °C) and had access to water and food ad libitum.

All experiments involving animals were conducted in strict accordance with the German animal welfare law, European legislation for the protection of animals used for scientific purposes (2010/63/EU), the Guide for the Care and Use of Laboratory Animals (part of the German Animal Welfare Law), and the Australian Code for the Care and Use of Animals for Scientific Purposes.

All scientific procedures on living animals were approved by the regional council (Regierungspräsidium Giessen GI 58/2014,GI20/25 No. G60/2017 and GI20/25 No. G71/2019) and the Monash Medical Centre Animal Experimentation Committee.

Induction of acute bacterial epididymitis in mice

Uropathogenic *Escherichia coli* (UPEC) strain CFT073[31] was obtained from the Institute of Medical Microbiology, Justus-Liebig-University Giessen, Germany. To induce ascending infection, the vasa deferentia were bilaterally ligated, followed by an intravasal injection of 5 µl sterile 0.9 % NaCl containing 1–2 × 10^5 colony-forming units proximal to the ligation using a Hamilton syringe (n = 3–7 per timepoint).[9] Control ('sham') mice underwent the same surgical procedure but received an intravasal injection of 5 µl sterile 0.9 % NaCl without bacteria (n = 3–7 per timepoint). Mice were sacrificed at specific time points after infection (1, 3, 5, 7, 10, 14, 21, and 28 days post-infection d.p.i.) using 4–5 % isoflurane inhalation followed by cervical dislocation (Suppl. Fig. 1A).

Induction of experimental-autoimmune epididymo-orchitis (EAEO)

To induce EAEO, adult male C57BL/6J mice were actively immunized with testicular homogenate (TH) in complete Freund's adjuvant (CFA; Sigma-Aldrich, St. Louis, USA), as previously described.[32–33] TH was prepared from decapsulated testes collected from adult mice and homogenized in sterile 0.9 % NaCl at a 1:1 ratio. Mice were immunized dorsally three times at 14-day intervals with a mixture of TH and CFA (200 µl total volume) delivered as four subcutaneous injections (50 µl per site). Subsequently, mice received an intraperitoneal injection of 100 ng *Bordetella pertussis* toxin (Calbiochem, Darmstadt, Germany) in 100 µl Munõz buffer (25 mM Tris, 0.5 M NaCl, 0.017 % Triton X-100, pH 7.6) (n = 11). Adjuvant control animals (n = 7) were administered CFA mixed with 0.9 % NaCl instead of TH, following the same injection protocol. Age-matched untreated mice (n = 7) were also included. Animals were sacrificed 50 days after the first immunization using 5 % isoflurane anaesthesia followed by cervical dislocation.

The epididymides and testes were removed, weighed, and either snap-frozen in liquid nitrogen or fixed in Bouin's solution for paraffin embedding. Fresh epididymides and testes were used for flow cytometric analysis.

Epididymides used for bulk RNA sequencing were collected from animals immunized at Monash University. Immunization protocols were modified per Monash University Animal Ethics Committee requirements, where mice received an initial immunization with TH in CFA, followed by two further immunizations with TH in incomplete Freund's adjuvant and *B. pertussis* toxin administration (n = 3). Adjuvant controls were also included (n = 3). Animals were euthanized using

Table 1
Andrological parameters of the study population of patients with acute epididymitis for serum CXCL13 measurement.

	Epididymal abscess (n = 10)	No abcess (n = 10)	*p* value
Patient demographics			
Age, yr, median (IQR)	65 (59–72)	63 (53–76)	0.880*
Side (right/left), *n* (%)	5/5 (50/50)	2/8 (20/80)	0.350‡
Indwelling catheter, *n* (%)	1 (10)	1 (10)	1.000†
Fever > 38 °C, *n* (%)	5 (50)	1 (10)	0.131‡
Patient history			
Onset of symptoms, d, median (IQR)	5 (2–6)	4 (3–7)	0.796*
Pain severity score, 0–10, median (IQR)	8 (3–8)	7 (5–8)	0.796*
Analgetic premedication, *n* (%)	4 (40)	3 (30)	1.000†
Antibiotic premedication, *n* (%)	4 (40)	5 (50)	1.000†
Urethritis, *n* (%)	0 (0)	0 (0)	1.000†
Dysuria, *n* (%)	4 (40)	1 (10)	0.303†
Endourological surgery within last 20 d, *n* (%)	0 (0)	2 (20)	0.474†
Respiratory tract symptoms within last 10 d, *n* (%)	0 (0)	0 (0)	1.000†
Sexually active within last 6 months, *n* (%)	3 (30)	5 (50)	0.650†
Sexual history suggestive of STIs, *n* (%)	0 (0)	0 (0)	1.000†
History of previous epididymitis, *n* (%)	0 (0)	0 (0)	1.000†
Laboratory findings			
WBC, giga/l, median (IQR)	10.8 (8.7–15.0)	12.0 (9.6–16.1)	0.436*
CRP, mg/l, median (IQR)	82.7 (28.5–155.7)	58.6 (18.0–109.1)	0.529*
PSA, ng/ml, median (IQR)	4.4 (2.1–9.9)	2.7 (0.6–6.1)	0.218*
Leukocytes, /µl urine, median (IQR)	500 (75–500)	500 (100–500)	0.965*
Urine microbiology			
E. coli	7	7	1.000‡
Enterococcus spp.	1	1	
Klebsiella spp.	1	1	
Setratia spp.	1	1	
Prostate ultrasound			
Transrectal ultrasound volume, ml, median (IQR)	27.6 (14.6–50.9)	22.4 (19.9–33.4)	0.897*
Local symptoms			
Scrotal wall induration, *n* (%)	3 (30)	1 (10)	0.582†
Epididymal pain on palpation, *n* (%)	10 (100)	10 (100)	1.000†
Testicular pain on palpation, *n* (%)	4 (40)	4 (40)	1.000†
Epididymal abscess in ultrasound, *n* (%)	10 (100)	0 (0)	**<0.001†**

WBC = white blood cell count; CRP = C-reactive protein; PSA = prostate-specific antigen. *Mann-Whitney *U* test. †Fisher's exact test. ‡Chi square test.

Table 2
Characteristics of patients suffering fulminant chronic epididymitis for histological and immunofluorescence analysis.

Age	Treatment	Pathologic Diagnosis
57	Epidiymectomy (left side)	Chronic epididymitis with acute immune response and spermatic granuloma of the left epididymis.
61	Epidiymectomy (left side)	Chronic inflammatory infiltration of the left epididymis
50	Epidiymectomy (right side)	Chronic inflammatory infiltration of the right epididymis

carbon dioxide overdose.

Human patient cohorts and ethical approval

Patients were retrospectively selected from the Giessen Epididymitis Study, a prospective study of male patients aged > 18 years on the etiology and clinical management of acute epididymitis, conducted between 2007 and 2023 at the Department of Urology, Pediatric Urology, and Andrology, Giessen, Germany (German Clinical Trials Registration DRKS00003325, institutional review board no. 100/7).

The inclusion criterion was acute epididymitis, defined as onset within the past 2 weeks, an enlarged epididymis on palpation typically associated with pain, and epididymal hyperemia on ultrasound.[1] A standardized and extensive microbiological workup was performed to identify common urinary tract pathogens as well as sexually transmittable diseases and viruses. Patients received a comprehensive standardized medical evaluation and were treated according to the current EAU guidelines.[34] Hospitalization was provided if clinically indicated. Primary antibiotic therapy included a fluoroquinolone, with the addition of a third-generation cephalosporin if necessary. Therapy was adjusted based on antimicrobial susceptibility testing results. Patients were offered follow-up evaluations at two weeks and three months. Clinical data and laboratory parameters were stored in a database (IBM SPSS, Ehningen, Germany). For the present study, 10 patients with epididymal abscesses were identified where the etiologically relevant pathogen was known, and follow-up data at 3 months post-treatment were available. Additionally, 10 patients without abscess formation, matched for age and bacterial pathogen, were included. Serum samples from nine men who had completed family planning and requested vasectomy were used as a comparison group, with written informed consent obtained. Detailed andrological parameters of the study population are shown in Table 1, and clinical course data are presented in Supplementary Table SI.

Histological Bouin-fixed tissue specimens (n = 3) from patients with chronic epididymitis undergoing semicastration at Shenzhen Second People's Hospital were also included (Table 2).[35] Semicastration was performed due to fulminant epididymitis with secondary testicular infarction in patients with scrotum pain exceeding one year, poor drug treatment efficacy response and completed family planning. Specimens of non-inflamed epididymal cauda regions used as controls were retrieved from two men (aged 23 and 33 years) undergoing orchiectomy due to testis cancer at the Department of Urology, Pediatric Urology, and Andrology, Giessen, Germany (Giessen Testis Cancer Patient Cohort). Histological samples were prepared following standard protocols and showed morphological intact, non-inflamed epididymal tissue without any signs of neoplastic infiltration. All patients provided written consent for the surgery and histological examination for research purposes.

Histological staining

Paraffin-embedded tissue sections from mouse and human epididymides were stained using routine Hematoxylin-Eosin, Masson-Goldner trichrome or azo-carmine and aniline blue (Azan) – staining.[36]

RNA extraction

RNA was extracted from the cauda epididymidis with a bead-based tissue homogenizer in QIAzol Lysis Reagent (Qiagen) or RLT buffer containing 1 % β-mercaptoethanol according to the manufacturer's protocol. The extracted RNA was processed using the RNeasy Mini Kit (Qiagen), and contaminating DNA was removed using the RNase-Free DNase Set (Qiagen). Samples were reverse-transcribed as previously described.[9] Quantitative reverse transcription-polymerase chain reaction (qRT-PCR) was performed using iTaq Universal SYBR Green Supermix (Bio-Rad, Munich, Germany) with in-house primers on a CFX96 Touch thermal cycler (Bio-Rad). Primer sequences and annealing temperatures are provided in Table 3. *Rplpo* was used as the housekeeping gene. All samples were run in duplicate. Relative mRNA expression levels were calculated using the $2^{-\Delta\Delta Ct}$ method.[37]

Table 3
Primers for qRT-PCR.

Gene	forward	reverse	Product size (bp)
Ccl19	ATGTGAATCACTCTGGCCCAGGAA	AAGCGGCTTTATTGGAAGCTCTGC	188
Ccl21	TGAGCTATGTGCAAACCCTGAGGA	TGAGGGCTGTGTCTGTTCAGTTCT	178
Cxcl13	GGCCACGGTATTCTGGAAGC	ACCGACAACAGTTGAAATCACTC	75
Glycam-1	TCAGCTGCAACCACCTCAG	TTCGTGATACGACTGGCACC	131
Lta	AGCCGTCAGATGACAACTAGG	CAAGCAGTGGCTGGCTTTTA	148
Ltb	AAAGACTGGATGACAGCAAA	GCTAGATTCCTGGAAGCATT	112
Rplpo	CTGCACTCTCGCTTTCTGGA	ACGCGCTTGTAGCCATTGAT	113
Tnf	CCCTCCTGGCCAACGGCATG	TCGGGGCAGCCTTGTCCCTT	109
Tnfs14	ATCAGGACCATGTTGGCAGG	GTGGCTGGAAACCAATGCAG	90

Table 4
Antibodies flow cytometric analysis.

Antibodies	Companies	Catalog No.	Clones	Final Dilution
Recombinant monoclonal anti-mouse CD19 PE-Vio770 REAfinity conjugated	Miltenyi Biotec, Bergisch Gladbach, Germany	130-112-037	REA749	1:50
Recombinant monoclonal anti-mouse CD138 APC REAfinity conjugated	Miltenyi Biotec	130-122-945	REA104	1:25
Recombinant monoclonal anti-mouse CD45 VioGreen REAfinity™ conjugated	Miltenyi Biotec	130-110-665	REA737	1:50
Recombinant monoclonal anti-mouse IgD FITC REAfinity™ conjugated	Miltenyi Biotec	130-111-495	REA772	1:50
Recombinant monoclonal anti-mouse IgM APC-Vio770 REAfinity conjugated	Miltenyi Biotec	130-116-315	REA979	1:50
Isotype control antibodies				
Recombinant monoclonal REA control PE-Vio770	Miltenyi Biotec	130-104-632	REA293	1:50
Recombinant monoclonal REA control APC	Miltenyi Biotec	130-104-630	REA293	1:25
Recombinant monoclonal REA control VioGreen	Miltenyi Biotec	130-104-624	REA293	1:50
Recombinant monoclonal REA control FITC	Miltenyi Biotec	130-113-437	REA293	1:50
Recombinant monoclonal REA control APC-Vio770	Miltenyi Biotec	130-104-634	REA293	1:50

Library preparation and RNA sequencing (RNA-Seq)

UPEC model

For genome-wide gene expression analysis, RNA sequencing libraries were generated and sequenced by the Institute for Lung Health– Genomics and Bioinformatics, Justus-Liebig-University Giessen, Germany. Polyadenylated mRNA was enriched from 200 ng of total RNA per sample using the NEBNext® Poly(A) mRNA Magnetic Isolation Module (New England BioLabs). Libraries were prepared using the NEBNext® Ultra™ II Directional RNA Library Prep Kit for Illumina® following the manufacturer's instructions. Library quality control was performed using capillary electrophoresis (4200 TapeStation, Agilent), and cDNA libraries were sequenced on an Illumina NovaSeq 6000 platform to generate 50 bp paired-end reads.

Sequencing reads were demultiplexed and converted to FASTQ files using Illumina software bcl2fastq (v2.19.0.316). Initial processing, including quality control, filtering, trimming, alignment, and gene-specific count table generation, was performed using the nf-core RNA-seq v3.7 bioinformatics pipeline[38] (NEXTFLOW version 23.04.03) with the *Mus* musculus mm10 genome and gene annotations from Illumina's iGenome repository (https://support.illumina.com/sequencing/sequencing_software/igenome.html). Default parameters were applied in Docker mode. Subsequent analyses, including normalization and differential gene expression detection, were performed in R using DESeq2.[39] Principal component analyses (PCAs) were calculated based on the top 500 most variable genes. Volcano plots were generated with the EnhancedVolcano R package.[40] ComplexHeatmap R packages were used for heatmap generation, respectively.[41] Differentially expressed genes (DEGs) were ranked by adjusted p-value, with the top 100 genes selected. Pathway enrichment and gene set analyses were performed using ClusterProfiler[42] against GO and Reactome databases. Raw sequencing data and the derived gene expression matrix were deposited in NCBI's Gene Expression Omnibus (GSE282584).

EAEO model

Total RNA concentrations were quantified using Qubit (Invitrogen), and quality was assessed with a Bioanalyzer (Agilent). RNA-seq transcriptomics were performed at the Hudson Genomics Facility (Melbourne, Australia). Libraries were prepared using an in-house multiplex RNA-seq method (version 01/09/2021) with 25 ng of total RNA input. An 8 bp i7 sample index and a 10 bp unique molecular identifier (UMI) were added during initial poly(A) priming, and pooled samples were amplified using a template-switching oligonucleotide. Illumina P5 and P7 adapters were added by tagmentation by Nextera transposase and PCR, respectively. Libraries were designed so that the forward read (R1) used the standard R1 primer to sequence cDNA in the sense direction for transcript identification. Samples were prepared as two libraries; the index read (I1) used the standard i7 primer to sequence directly into the sample index and then the 10 bp UMI, and an additional index read (I2) sequenced the i5 library index. Sequencing was performed on a NextSeq 2000 platform, as per the manufacturer's instructions (Illumina) using a P3 50 cycle kit (R1: 61 bp; I1: 18 bp; I2: 8 bp). On-board denaturing and clustering were performed using 900 pM of the library pool, following Illumina Protocol 1,000,000,109,376 v3 (Nov 2020). Base calling was carried out using Dragen BCLConvert (v3.7.4).

Data processing was automated using the RNAsik pipeline.[43] Differential expression analysis was performed on the Degust platform with the Voom-limma method.[44] A permissive threshold was applied for defining significantly differentially expressed genes in EAEO groups compared to the control group (cut off: absolute log fold change [absLog2FC] > 0.585, false discovery rate [FDR] < 0.05).

Flow cytometry

Pooled proximal regions and cauda epididymides were digested in PBS containing 1.5 mg/ml collagenase A (Roche Diagnostic, Mannheim, Germany) for 45 min at 37 °C to generate single cell suspensions as

Table 5
Primary and secondary antibodies for immunofluorescence staining.

Antibodies/ Lectin	Company	Catalog No.	Dilution
Rat monoclonal anti-AID	Invitrogen, Oregon, USA	14-5959-82	1:30
Rat monoclonal anti-CD138	BioLegend, San Diego, CA, USA	142501	1:100
Rabbit monoclonal anti-CD19	Abcam, Cambridge, UK	ab245235	1:50
Rat monclonal anti-CD3ε	Cell Signaling Technology, Danvers, Massachusetts, USA	4443	1:50
Rabbit monoclonal anti-CD45	Cell Signaling Technology	D3F8Q	1:50
Goat polyclonal anti-CXCL13	R&D Systems, Minneapolis, Minnesota, USA	PA5-47018	1:20
Rat monoclonal anti-F4/80	Cell Signaling Technology	71299	1:100
Rat monoclonal anti-MECA-79	BioLegend, San Diego, CA, USA	120801	1:100
Rat monoclonal anti-MECA-79 Alexa Fluor 647	BioLegend	120807	1:100
Mouse monoclonal anti-PCNA	BioLegend	307901	1:50
Goat polyclonal anti-podoplanin	R&D Systems, Minneapolis	AF3244	1:20
Mouse monoclonal anti-CD45	Dianova GmbH, Hamburg, Germany	DLN-083890	1:30
Mouse monoclonal anti-CD20cy	Agilent Technologies, Santa Clara, CA, USA	M075501-2	1:50
Rabbit polyclonal anti-CD3	Agilent	A045229-2	1:50
Pure *Arachis hypogaea* lectin (PNA), FITC conjugated	EY Laboratories, San Mateo, USA	F-2301-1	1:200
Secondary Antibodies			
Goat anti-rat IgG (H + L) Alexa Fluor 546 conjugated	Invitrogen, Oregon, USA	A-11081	1:2000
Goat anti-rabbit IgG (H + L) Alexa Fluor 488 conjugated	Invitrogen	A-11034	1:2000
Goat anti-rabbit IgG (H + L) Alexa Fluor 546 conjugated	Invitrogen	A-11008	1:2000
Goat anti-rat IgG (H + L) Highly Cross-Adsorbed Alexa Fluor 488 conjugated	Invitrogen	A48262	1:1000
Donkey anti-goat (H + L) Alexa Fluor 488 conjugated	abcam	ab150129	1:1000
Donkey anti-mouse IgG (H + L) Highly Cross-Adsorbed Alexa Fluor 488 conjugated	Invitrogen	A21202	1:1000
Donkey anti-rat IgG (H + L) Highly Cross-Adsorbed Alexa Fluor Plus 647 Conjugated	Invitrogen	A48272	1:500
Goat anti-mouse IgG F(ab)2 Alexa Fluor 488 conjugated	Jackson ImmunoResearch Labs, West Grove, USA	115-546-072	1:800

described earlier.[9] The resulting cell suspension was vortexed, passed through a 20G needle, and filtered through a 70 μm strainer. After washing with PBS, the cells were centrifuged at 300*g* for 10 min. The testes were processed as described earlier.[32] Briefly, decapsulated testes were digested in 1.2 mg/ml collagenase A (Roche Diagnostic, Mannheim, Germany) and 15 U/ml DNase I (Roche Diagnostic) in a 34 °C water bath for 15 min. Supernatants containing interstitial cells were then collected. A total of 1×10^6 cells were resuspended in PBS and stained with Fixable Viability Dye eFluor 450 (Thermo Fisher Scientific) for 30 min at 4 °C in the dark. Cells were then centrifuged and incubated with mouse FcR blocking reagent (Miltenyi Biotec) for 10 min at 4 °C, followed by staining with appropriate antibodies for 20 min at room temperature in the dark (Table 4). After staining, cells were washed, centrifuged, and resuspended in MACSQuant buffer for flow cytometry measurement using the MACSQuant Analyzer 10. Data analysis was performed using FlowJo v10 software (FlowJo LLC, Ashland, OR, USA). The gating strategy is shown in Suppl. Fig. 2.

Immunofluorescence staining in mouse and human paraffin sections

Paraffin-embedded tissue sections were stained using immunofluorescence with specific antibodies for markers and factors important for TLO composition. Sections were deparaffinized, rehydrated, and subjected to antigen retrieval using either sodium citrate buffer (10 mM, pH 6.0) or proteinase K (0.6 units/ml in TE buffer, pH 8.0). Specific antibodies (Table 5) were applied, followed by incubation with appropriate secondary antibodies. After washing, sections were treated with 0.3 % Sudan Black in 70 % ethanol for 5 min to reduce autofluorescence, followed by mounting with ProLong Gold Antifade Mountant containing DAPI (Thermo Fisher Scientific). All antibodies were diluted in TBS. Negative controls, omitting the primary antibody, showed no immunofluorescence signal (Suppl. Fig. 3). Furthermore, positive controls for immunostainings were included using tissues with a known pattern of respective protein expression (Suppl. Fig. 4). Results confirmed the expected localization and signal intensity, supporting the validity of the staining protocol. Fluorescence images were taken using confocal laser scanning microscope 710 (Carl Zeiss, Göttingen, Germany) and Stellaris 5 (Leica Microsystems, Wetzlar, Germany) or Leica Thunder wide field fluorescence microscope (Leica Microsystems).

ELISA CXCL13 human serum

The concentration of CXCL13 in sera from epididymitis patients and healthy controls was measured using the Human CXCL13 (BCA-1) ELISA Kit (Abcam, Cambridge, United Kingdom) following the manufacturer's instructions. Optical density was measured at 450 nm using a Tristar LB 941 Microplate Reader (Berthold Technologies, Bad Wildbad, Germany).

Statistical analyses

Statistical analyses were conducted using GraphPad Prism 10 (GraphPad Software, San Diego, CA, USA). Data are presented as mean ± standard error of the mean (SEM). Normal distribution and equal variance were assessed prior to analysis. Differences between two groups were evaluated using Student's *t*-test (for Gaussian distributions) or Mann-Whitney test (for non-parametric distributions). For comparisons involving multiple groups, one-way or two-way ANOVA with Tukey's post-hoc test (Gaussian distributions) or Kruskal-Wallis tests with Dunn's post-hoc comparisons (non-parametric distributions) were applied. A p-value < 0.05 was considered statistically significant.

The demographics and characteristics of epididymitis patients with and without epididymal abscess formation were compared using the Mann-Whitney *U* test, Fisher's exact test, or chi-square test, as appropriate. Variables are reported as medians and interquartile ranges (IQR) or as numbers and percentages. Statistical analyses were conducted using SPSS v22 for Windows (IBM GmbH, Ehningen, Germany).

Results

Tertiary lymphoid organ elements develop in the cauda epididymidis at late stages following mouse UPEC infection

The mechanisms underlying disturbances in spermatogenesis and the

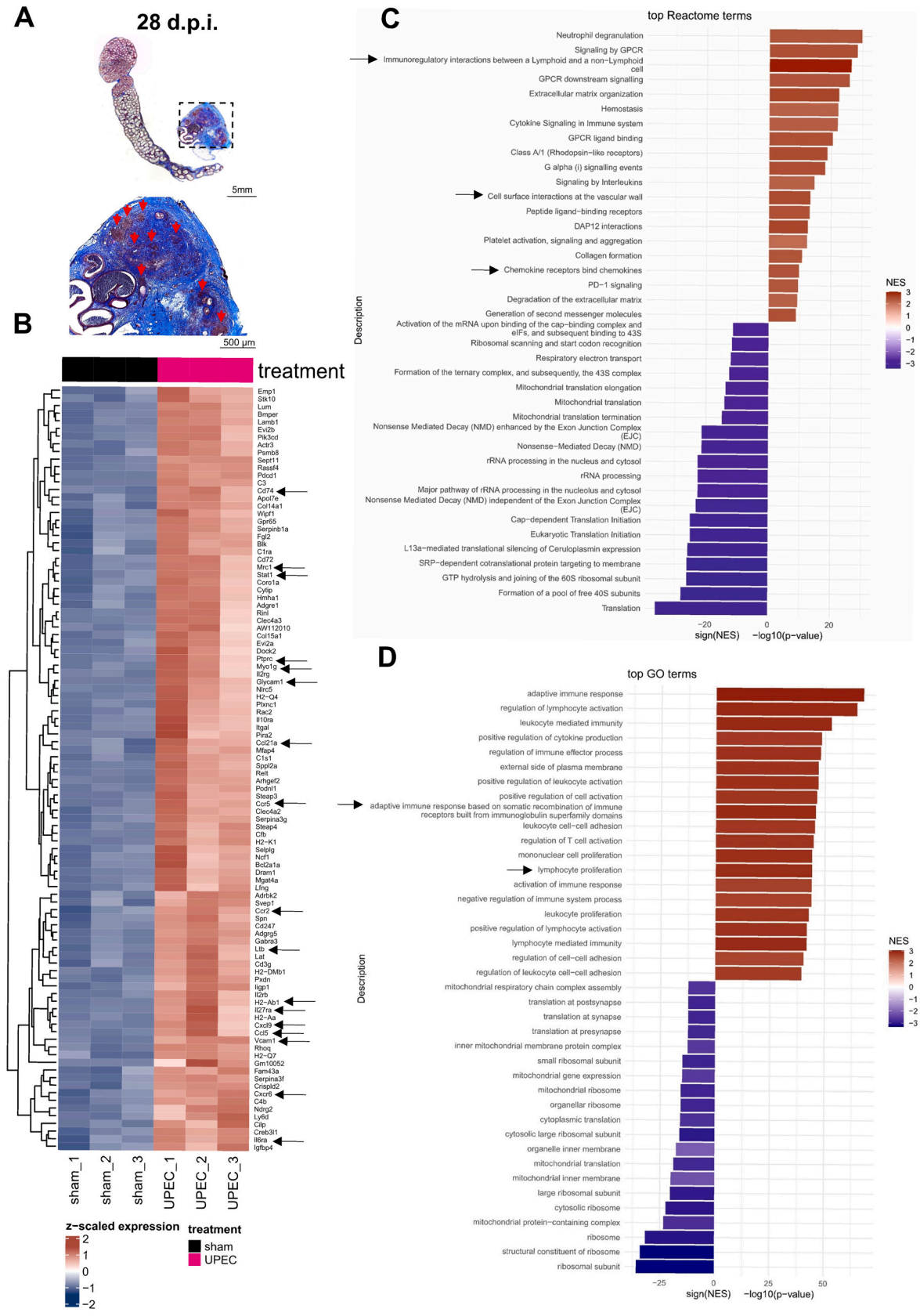


Fig. 1. Upregulated genes and pathways involved in tertiary lymphoid organ formation and maintenance 28 days post mouse UPEC infection. Representative photomicrograph of Azan staining in paraffin sections of cauda epididymides 28 days post-infection (d.p.i.), with arrows indicating organized immune cell clusters (A). Heatmap of z-transformed expression values for the top 100 upregulated genes (ranked by p-value) in UPEC-infected vs sham cauda epididymidis at 28 d.p.i. (B). Top 20 upregulated and downregulated Reactome pathways (C) and GO terms (D) identified by gene set enrichment analysis (GSEA) of differentially expressed genes (DEGs) in sham vs UPEC-infected cauda epididymidis 28 d.p.i.

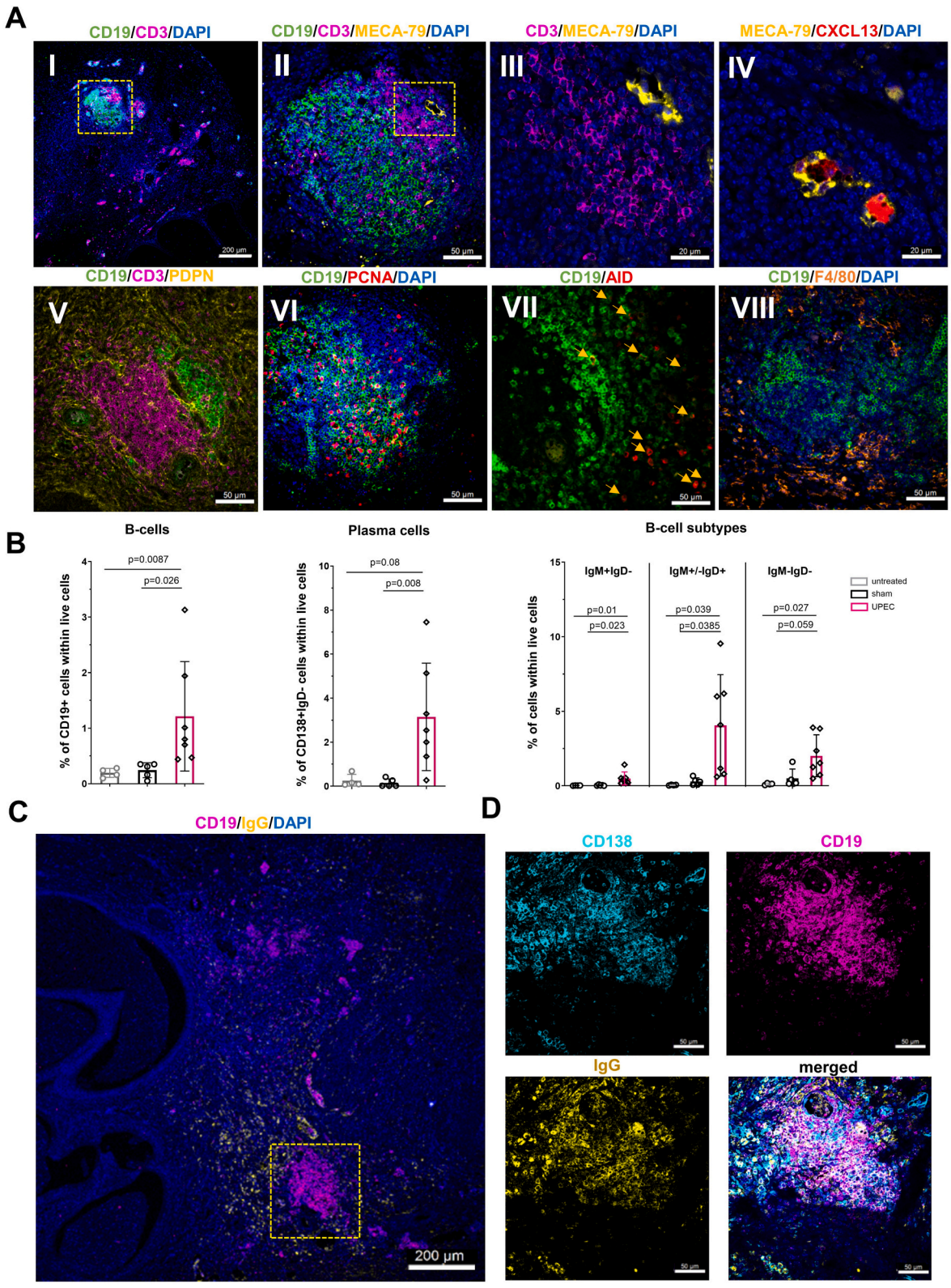


Fig. 2. Tertiary lymphoid organs in UPEC-infected mouse cauda epididymidis at 28 d.p.i. exhibit germinal centers, diverse B-cell subsets, and local immunoglobulin production. Representative photomicrographs showing immunofluorescence staining for CD19 (green; I, II, V – VIII), CD3 (pink; I – III, V), PDPN (yellow; V), MECA-79 (yellow; II – IV), CXCL13 (red; IV), PCNA (red; VI), AID (red; VII) and F4/80 (orange; VIII), with nuclei stained with DAPI (blue) in mouse cauda epididymidis at 28 d.p.i. (A). Percentages of $CD45^{+}CD19^{+}$ B-cells, $CD45^{+}CD19^{-}IgD^{-}CD138^{+}$ plasma cells, and isotype-switched B-cells ($CD45^{+}CD19^{+}IgM^{+}IgD^{-}$, $CD45^{+}CD19^{+}IgM^{+/-}IgD^{-}$, $CD45^{+}CD19^{+}IgM^{-}IgD^{-}$) in untreated, sham, and UPEC-infected cauda epididymides at 28 d.p.i. were quantified by flow cytometry (n = 4–7; mean ± SEM). Statistical analyses used one-way ANOVA with Tukey's post-hoc test or Kruskal-Wallis tests with Dunn's post-hoc comparisons (B). Representative photomicrographs of IgG (yellow), CD138 (turquoise), CD19 (pink) immunofluorescence, and DAPI-stained nuclei (blue) in cauda epididymidis 28 d.p.i. (C, D). (For interpretation of the references to colour in this figure legend, the reader is referred to the web version of this article.)

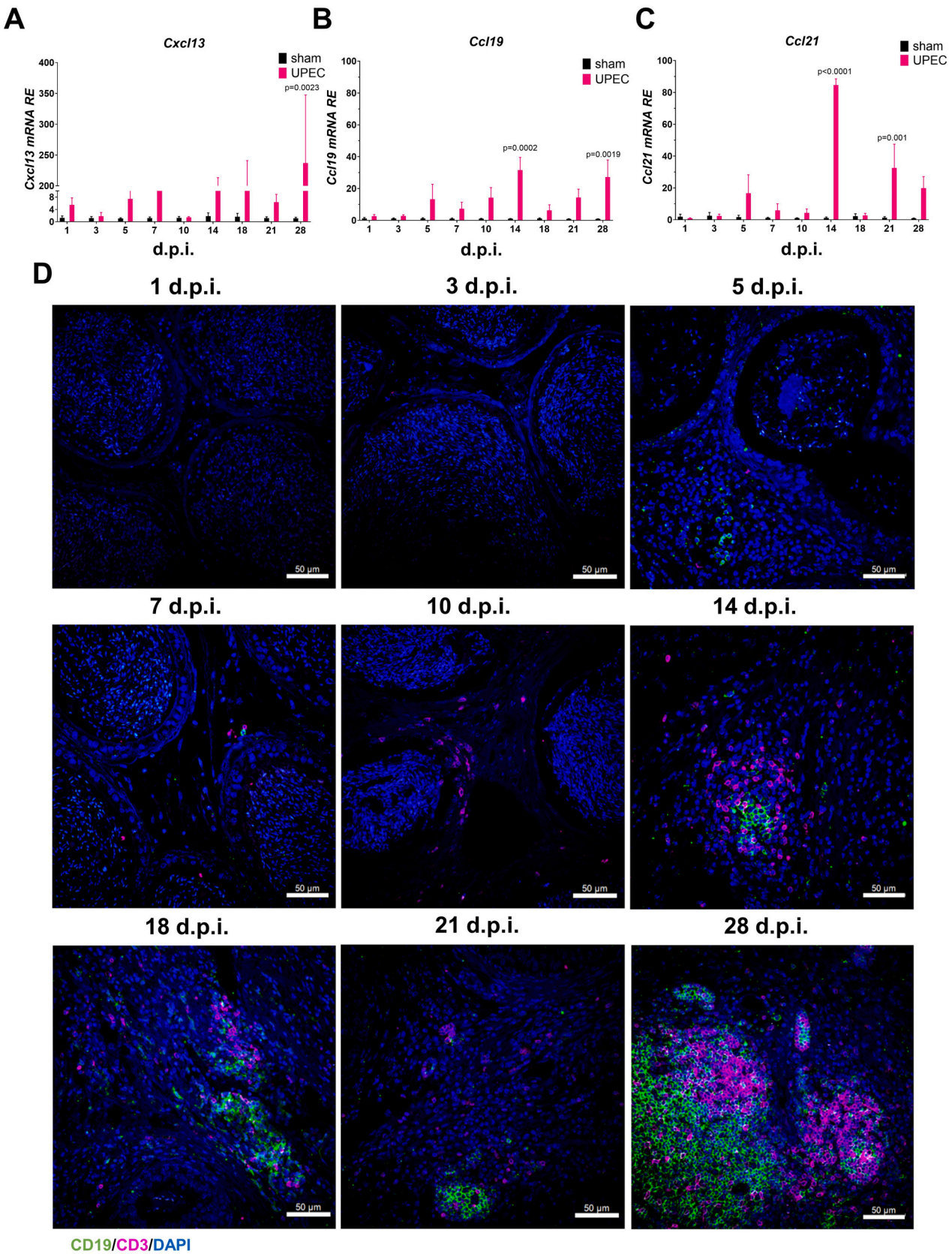


Fig. 3. Expression of lymphoid chemokines supports B- and T-cell compartmentalization in UPEC-infected mouse cauda epididymidis. Relative expression (RE) of *Cxcl13* (A), *Ccl19* (B), and *Ccl21*(C) mRNA was measured by qRT-PCR in sham and UPEC-infected cauda epididymides at 1, 3, 5, 7, 10, 14, 18, 21, and 28 d.p.i., normalized to *Rplpo* (n = 3; mean ± SEM). Statistical analysis used two-way ANOVA followed by Tukey's test. Representative photomicrographs showing immunofluorescence staining for CD19 (green), CD3 (pink) and nuclei (DAPI, blue) in cauda epididymidis at 1, 3, 5, 7, 10, 14, 18, 21and 28 d.p.i. (D). (For interpretation of the references to colour in this figure legend, the reader is referred to the web version of this article.)

formation of epididymal abscesses following acute epididymitis in men remain poorly understood.[1,3] To address this issue, we investigated the post-acute and chronic stages of the disease. As biopsies in bacterial epididymitis patients are contraindicated, we utilized a well-established mouse model of bacterial epididymitis to analyze the cauda epididymidis 28 days post-infection (d.p.i.) (Suppl. Fig. 1A). Histological analysis revealed smaller abscesses in the cauda epididymidis at 28 d.p.i. compared to earlier time points (10 and 14 d.p.i.) (Fig. 1A, Suppl. Fig. 1B, C). However, multiple small immune aggregates that were well organized and accompanied by collagen deposition were observed at the terminal part of the epididymis 28 d.p.i. (Fig. 1A). Given the organized structure of the clusters, we sought to investigate their nature further by performing transcriptomic analysis at the same time point. Among the top 100 differentially expressed genes (DEGs) in the cauda epididymidis at 28 d.p.i. (vs. sham-operated controls), most highly upregulated genes were associated with immune response and inflammation (e.g., *Ccl5, Cd74, Cxcl9, H2-Aa, H2-Ab1, Il6ra, Il2rb, Ltb, Mrc1, Stat1*), cell adhesion and trafficking (e.g., *Ccr2, Ccr5, Cxcr6, Ccl21a, Myo1g, Ptprc, Vcam1*), and HEV formation (including *Glycam-1,* which encodes a proteoglycan ligand expressed on HEVs in lymphoid tissue[22] (Fig. 1B). Analysis of the top 20 upregulated pathways using the GO and Reactome databases highlighted gene sets associated with 'immunoregulatory interactions between a lymphoid and non-lymphoid cell,' 'cell surface interactions at the vascular wall,' and 'chemokine receptors bind chemokines' (Fig. 1C, Suppl. Fig. 5A–C, Suppl. Table SII). Other highly upregulated pathways included 'lymphocyte proliferation' and 'adaptive immune response based on somatic recombination of immune receptors built from immunoglobulin superfamily domains' (Fig. 1D, Suppl. Fig. 5D, E, Suppl. Table SIII). In contrast, the downregulated gene sets in our study were associated with metabolism and biosynthesis (e.g., *Alad, Cyp51, Fdps, Ptgs1, Gstm1, Gstm7, Msmo1, Fdft1*), structure and motility (e.g., *Camsap3, Dtnb, Map1lc3a, Trim2*), as well as signaling (e.g., *Efna4, Erbb2, Mapk3a, Pax2, Wnt4,*) (Suppl. Fig. 5F). These findings indicate the potential formation of TLO and germinal centre activity in the cauda epididymidis following *UPEC* infection, warranting further investigation.

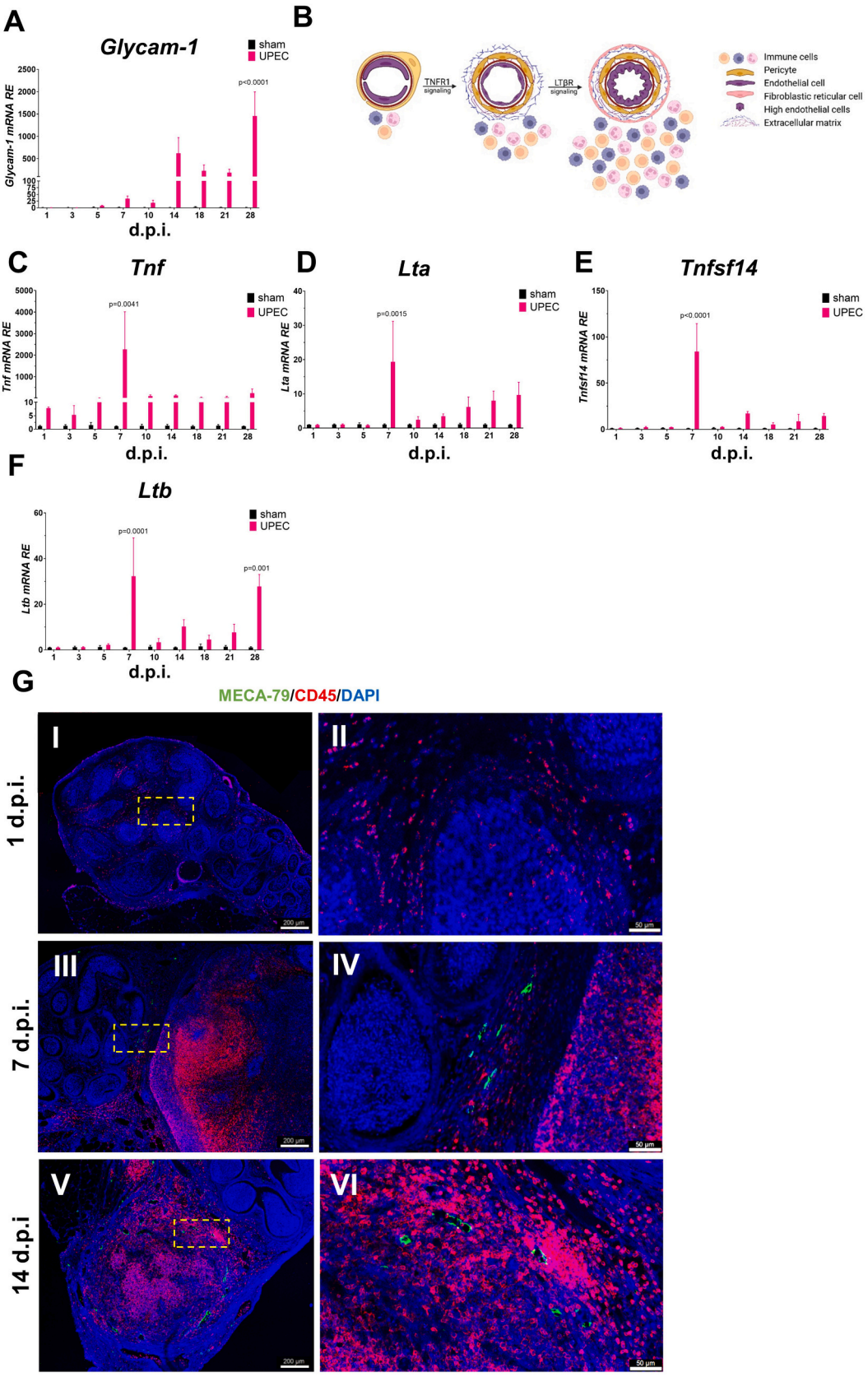
To visually confirm the formation of TLOs in the infected cauda epididymidis, we performed an immunofluorescence analysis to define the immune cell composition of cell clusters. At 28 d.p.i., we detected immune cell infiltrates that were predominantly organized into clusters of B- and T-cells with distinct zones (Fig. 2AI–II, Suppl. Fig. 6A). Notably, lymphocyte clusters were detected exclusively in the cauda epididymidis and not in the proximal regions of epididymis at 10, 14 or 28 d.p.i. (Suppl. Fig. 7A, C, E). The B and T cell clusters also contained podoplanin (PDPN), a marker of lymphoid stromal cells (Fig. 2AV, Suppl. Fig. 6C), indicating the development of a supportive, reticular network within these aggregates. Lymphoid stromal cells provide structural support and spatial arrangement of lymphoid immune cells as well as a reticular network for the lymphoid organ.[45–46] Importantly, MECA-79 staining revealed HEVs localized within T-cell zones (Fig. 2AII-III) and containing CXCL13 within their lumen (Fig. 2AIV, Suppl. Fig. 6B). We also detected proliferating B-cells, present only at 28 d.p.i., but not at 14 or 18 d.p.i., indicative of cells capable of producing high-affinity antibodies (Fig. 2AVI; Suppl. Fig. 6D). Moreover, within the immune cell aggregates, we found cells expressing activation-induced cytidine deaminase (AID) (Fig. 2AVII, Suppl. Fig. 6E), that is specifically expressed in germinal center B cells and is involved in somatic hypermutation, gene conversion, and class-switch recombination of immunoglobulin genes.[47] Surrounding the B-cell clusters were F4/80$^+$ macrophages (Fig. 2AVIII), which typically function as antigen-presenting cells and influence B-cell survival and proliferation.[48] None of the cellular components specific for TLO organization mentioned above were observed in sham treated controls at 28 d.p.i. (Suppl. Fig. 8). These findings demonstrate that the immune cell clusters in the cauda epididymidis are, in fact, organized lymphoid structures, that display advanced characteristics of a TLO.

TLOs in the mouse cauda epididymidis exhibit germinal centers and B-cell diversity

SLOs contain germinal centers (GCs), which are hubs for B-cell selection and affinity maturation and can also develop in TLOs.[49] We investigated whether GCs were present in the TLOs of the cauda epididymidis in our mouse model by examining their capacity to activate molecular pathways required for the *in situ* differentiation of class-switched, antibody-producing B-cells. Flow cytometry revealed significantly increased percentages of B-cells in the cauda epididymidis at 28 d.p.i. compared to untreated and sham mice (Fig. 2B, Suppl. Fig. 9). Moreover, the percentage of CD138$^+$IgD$^-$ plasma cells was significantly increased in the UPEC cauda epididymis compared to sham controls at 28 d.p.i. (Fig. 2B, Suppl. Fig. 9). The analyzed B-cell subtypes included IgM$^+$IgD$^-$ (earliest stage of B-cells detectable outside the bone marrow), IgM$^{+/-}$IgD$^-$ (mature B-cells), and IgM$^-$IgD$^-$ (mature, activated, specialized B-cells, including isotype-switched or germinal centre B-cells)[50] (Fig. 2B, Suppl. Fig. 7, 10). In contrast, in the proximal regions of the epididymis (initial segment and caput), the number of B-cells was slightly increased, showing only a minor elevation in IgM$^-$IgD$^-$ subpopulation compared to UPEC infected cauda epididymidis (0.5 % vs 2.5 %) (Suppl. Fig. 7B, D, F). Interestingly, at 10 and 14 d.p.i, the percentage of B-cells remained unchanged in the UPEC-infected cauda. However, a slight increase was observed in UPEC-infected proximal parts starting at day 14 and continuing through 28 d.p.i., accompanied by a concomitant rise in the IgM$^-$IgD$^-$ subpopulation. Notably, the IgM$^-$IgD$^-$ subpopulation was significantly upregulated at 14 d.p.i. in the UPEC-infected cauda (Suppl Fig. 7B, D, F, Suppl. Fig. 10). In contrast, this population remained unchanged in the proximal regions at 10 and 14 d.p.i (Suppl. Fig. 7). Furthermore, no detectable B and T cells clusters were present in the proximal epididymis at any of the time points investigated (Suppl. Fig. 7A, C, E). Using triple immunofluorescence staining for immunoglobulin G (IgG), B-cells (CD19), and plasma cells (CD138), we demonstrated the presence of IgG$^+$ B-cells and IgG$^+$ plasma cells in the cauda epididymidis at 28 d.p.i. (Fig. 2C-D). The spatial organization of B-cells surrounded by isotype-switched plasma cells suggests that these plasma cells were generated in GCs formed within the cauda epididymidis (Fig. 2C-D). Our earlier evidence of B-cell proliferation (Fig. 2AVI, Suppl. Fig. 6D) and AID expression (Fig. 2AVII, Suppl. Fig. 6E) further supports this conclusion, and it aligns with our transcriptomic data showing upregulation of genes associated with lymphocyte proliferation and adaptive immune responses based on somatic recombination of immune receptors from immunoglobulin superfamily domains (Fig. 1D). We thus conclude that functionally active GCs form in the TLOs of the cauda epididymidis by 28 d.p.i.

TLOs are absent from the mouse cauda epididymidis during the acute phase of infection

To investigate the dynamics of TLO formation during murine epididymitis, we examined the presence of TLO mediators during the acute and chronic course of infection at 1, 3, 5, 7, 10, 14, 18, 21, and 28 d.p.i. A key criterion for TLOs is the presence of T- and B-cell-rich areas, which, in advanced stages, are segregated into distinct zones.[15,22,51] The recruitment and compartmentalization of T- and B-cell zones within lymphoid tissues is partially driven by gradients of chemokines CXCL13 (a B-cell chemoattractant), CCL19, and CCL21.[15,19] To assess this, we analyzed lymphoid chemokine gene expression in the cauda epididymidis of UPEC-infected mice compared to sham-operated controls over the course of infection. At 1 d.p.i., there was a 5-fold increase in *Cxcl13* in UPEC infected cauda epididymidis compared to sham controls, which was not observed in the other chemokines at this time point. We detected a significant peak in *Ccl19* and *Ccl21* mRNA expression (approximately 30- and 70-fold increase, respectively) at 14 d.p.i., and a coincident peak of *Cxcl13* expression (~150-fold) that did not achieve significance at $p < 0.05$ due to high variability (Fig. 3A–C). At 21 d.p.i.,



(caption on next page)

Fig. 4. High endothelial venules (HEVs) form in the mouse cauda epididymidis post-UPEC infection. Relative expression (RE) of *Glycam-1* mRNA was measured by qRT-PCR in sham and UPEC-infected cauda epididymides at 1, 3, 5, 7, 10, 14, 18, 21, and 28 d.p.i., normalized to *Rplp*o (n = 3; mean ± SEM). Statistical analysis used two-way ANOVA followed by Tukey's test (A). Schematic illustration of mechanisms driving HEV formation and maturation, showing sequential stages from venule modification to fully mature HEVs. HEVs develop from post-translational modifications of normal venules lacking MECA-79 expression that recruit few immune cells. Under inflammatory conditions, TNFR1 pathway activation via lymphotoxin (LT) α3 signaling changes the normal venule into an immature HEV with flat endothelial cells. Prolonged inflammatory signals stimulate the LT β receptor (R) pathway, which allow the HEV to acquire a mature phenotype. A mature HEV possesses cuboidal endothelial cells, is enclosed by concentric layers of fibroblastic reticular cells (FRC) and can recruit large numbers of lymphocytes. Figure created with BioRender (B). Relative expression (RE) of *Tnf* (C), *Lta* (D), *Tnfs14* (E), and *Ltb* (F) mRNA was analyzed in sham and UPEC-infected cauda epididymides by qRT-PCR as in (A) (n = 3; mean ± SEM). Representative photomicrographs of CD45 (red), MECA-79 (green), and nuclei (DAPI, blue) in cauda epididymidis at 1 (I, II), 7 (III, IV), and 14 (V, VI) d.p.i. (G). (For interpretation of the references to colour in this figure legend, the reader is referred to the web version of this article.)

Ccl21 reached another peak (~30-fold increase), while *Ccl19* and *Cxcl13* peaked again (~ 25- and 250-fold increase, respectively) at 28 d.p.i. (Fig. 3A–C). These findings suggest that B- and T-cell recruitment, as well as potential compartmentalization, begins by 14 d.p.i. Immunofluorescence staining confirmed this hypothesis, showing only small B-cell clusters at 5 d.p.i., and clusters of both B- and T-cells at 14, 18 and 21 d.p.i. that were smaller than the well-organized clusters observed at 28 d.p.i. (Fig. 3D).

HEVs are detectable in the mouse cauda epididymidis at multiple time points

In our histopathological analysis, we observed massive immune cell infiltrates in the mouse cauda epididymidis at 10 and 14 d.p.i., but not in the proximal regions (Suppl. Fig. 1**B, C)**. In addition, we detected increased *Glycam-1* gene expression (Fig. 1B) and the presence of MECA-79$^+$ cells at 28 d.p.i., indicative of HEVs (Fig. 2AII, III, IV). We hypothesized that the immune cells forming abscesses could be recruited via HEVs during the acute phase of the infection. To investigate the presence of HEVs at earlier time points, we analyzed *Glycam-1* mRNA expression throughout the infection. A rise of *Glycam-1* gene expression was apparent at 7 d.p.i. (approximately 25-fold increase), followed by further elevated expression at 14 d.p.i., reaching a significant peak at 28 d.p.i., (~500- and 1500-fold increase, respectively) (Fig. 4A). These findings indicate that HEVs may begin to form as early as 7 d.p.i.

HEV formation can be initiated by tumor necrosis factor receptor 1 (TNFR1) signaling, while HEV maturation requires activation of the lymphotoxin beta receptor (LTβR)[22] (Fig. 4B). To understand the mechanisms guiding the ectopic formation of HEV, we measured the expression of HEV mediators, involved in their formation as well maturation in the mouse cauda epididymidis during early and chronic phase of infection. The expression of *Tnf, Lta, Tnfsf14,* and *Ltb,* mediators for HEV formation and maturation acting through TNFR1 and LTβR pathway (Fig. 4B), peaked significantly (approximately 2000-, 20-, 100- and 30-fold increase, respectively) at 7 d.p.i and had declined by 10 d.p.i. (Fig. 4C–F). A second significant peak in *Ltb* expression (~ 30-fold increase) was detected at 28 d.p.i. (Fig. 4F), suggesting ongoing HEV development and functional maturation from 7 d.p.i. No HEVs were detected at 1 d.p.i. as confirmed by MECA-79 immunostaining (Fig. 4GI–II). The presence of HEV-like vessels near immune cell infiltrates was observed at 7 d.p.i. (Fig. 4GIII–IV), with higher density of infiltrates at 14 d.p.i. (Fig. 4GV–VI). These results align with the peaks in HEV-related gene expression and massive immune cell infiltrates at 7 and 14 d.p.i. (Fig. 4GIII–VI). We posit that HEVs likely facilitate immune cell recruitment to the UPEC-infected cauda epididymidis, and that the formation of massive abscesses post-infection might be a consequence of HEV development.

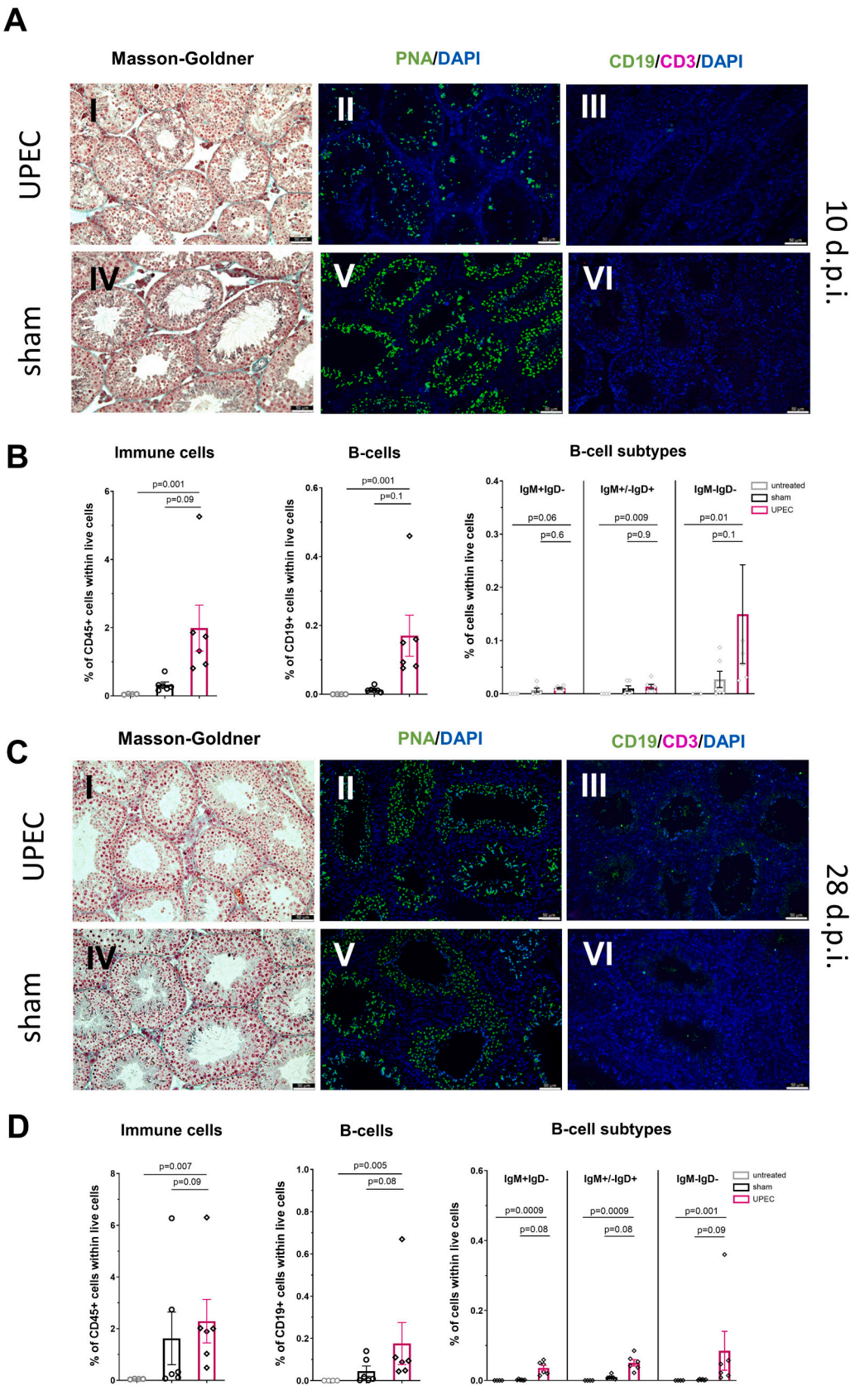
TLO are not present in testis post UPEC infection

To investigate potential disturbances in spermatogenesis and the presence of TLOs in the testis during chronic UPEC induced epididymitis, we examined the testicular architecture, acrosome formation, cellular components associated with TLOs and B cell diversity at 10 and 28 d.p.i. We selected 10 d.p.i. as a key time point based on previous reports indicating early spermatogenic impairment at this stage.[52] Histological staining revealed several pathological alterations in the seminiferous tubules at 10 d.p.i. including germ cell loss, reduced epithelial thickness and vacuolisation of the germinal epithelium (Fig. 5AI). FITC – conjugated Peanut agglutinin (PNA) staining of the acrosomes by showed a decreased presence of mature acrosomes in most spermatozoa within the seminiferous tubules following UPEC infection at 10 d.p.i. (Fig. 5AII). In contrast, by 28 d.p.i., the testicular architecture had largely recovered (Fig. 5CI), and normal acrosome formation was observed (Fig. 5CII). Sham treated mice displayed normal testicular histology and presence of acrosomes both at 10 and 28 d.p.i. (Fig. 5AIV, V, 5CIV, V). Flow cytometric analysis of immune cells and B-cell subsets revealed a significant increase in CD45$^+$ cells, B-cells and IgM$^-$IgD$^-$ subpopulation at 10 and 28 d.p.i in UPEC testes as compared to untreated, but not sham controls (Fig. 5B, D; Suppl. Fig. 11). Of note, the testis from sham treated mice demonstrated slightly elevated percentage of CD45$^+$ cells and B-cells at 10 and 28 d.p.i (Fig. 5B, D). Therefore these effects seem to be related to the surgical procedure causing minimal immune response. Despite this slight immune cell infiltration in UPEC group, no clusters of B- and T-cells were detected within the testicular parenchyma at either time point (Fig. 5AIII, CIII). These data indicate that there is no evidence for the formation of TLOs in the UPEC infected testes at 10 and 28 d.p.i.

Elements of TLO are also present in the inflamed mouse cauda epididymidis under autoimmune conditions

To further investigate the susceptibility of the cauda epididymidis to TLO formation, we examined this process under chronic, sterile autoimmune conditions using a well-established mouse model of experimental autoimmune epididymo-orchitis (EAEO) (Fig. 6A). In this model chronic inflammation is induced by active immunization with testicular homogenates leading to destruction of spermatogenesis, fibrotic remodeling and development of epididymitis.[32–33,53] Similar to acute bacterial epididymitis, the proximal regions of the epididymis remained unaffected in EAEO, while the cauda epididymidis exhibited severe inflammatory and fibrotic reactions.[53] In EAEO mice, the cauda epididymidis displayed immune cell infiltrates alongside fibrotic remodeling, consistent with previous findings[53] (Fig. 6B). MECA-79$^+$ HEVs were also detected in the cauda epididymidis and were associated with clusters of B-cells intermingled with T-cells (Fig. 6CI, II).

In contrast to the UPEC-infected cauda epididymidis, the B-cells in EAEO cauda epididymidis did not proliferate, and PDPN expression was absent within the B-cell clusters, indicating a lack of a reticular network in these lymphoid aggregates (Fig. 6CIII–IV). Additionally, the B- and T-cell clusters in EAEO mice were not well-segregated into distinct zones. While *Cxcl13* (~ 15-fold) and *Ccl19* (~6-fold) mRNA expression was increased, *Ccl21* expression did not increase significantly compared to controls (Fig. 6D). These findings suggest that the absence of B- and T-



(caption on next page)

Fig. 5. Tertiary lymphoid organs are not present in testis post UPEC infection. Representative photomicrographs of Azan staining (I, IV), PNA (green) and DAPI (blue) immunofluorescence staining (II, V) and of CD19 (green) and CD3 (pink) with DAPI (III, VI) in paraffin sections from UPEC-infected and sham testis at 10 d.p.i. (A) and at 28 d.p.i. (C). Percentages of $CD45^+$ immune cells and $CD45^+CD19^+$ B-cells as well as isotype-switched B-cells ($CD45^+CD19^+IgM^+IgD^-$, $CD45^+CD19^+IgM^{+/-}IgD^-$, $CD45^+CD19^+IgM^-IgD^-$) in untreated, sham, and UPEC testes were determined by flow cytometry at 10 d.p.i (B) and 28 d.p.i (D); n = 4–6; mean ± SEM). Statistical analysis used Kruskal–Wallis test followed by Dunn's multiple comparison test. (For interpretation of the references to colour in this figure legend, the reader is referred to the web version of this article.)

cell compartmentalization may result from insufficient expression of TLO-related chemokines, such as *Ccl21*.

Given the presence of HEVs in EAEO cauda epididymidis, we analyzed the mediators involved in their ectopic formation. Expression of *Tnf, Lta, Tnfsf14* and *Ltb* mRNA was significantly increased (approximately 30-, 7.5-, 4-, 15-fold, respectively) in EAEO cauda epididymidis compared to controls (Fig. 6D). These changes were accompanied by an increased percentage of B-cells in EAEO cauda epididymidis compared to controls (Fig. 6E). Similar to UPEC infected cauda epididymides, the percentage of plasma cells and investigated B cell subtypes (IgM^+IgD^-, $IgM^{+/-}IgD^-$ and IgM^-IgD^-) was significantly increased compared to control mice (Fig. 6E, Suppl. Fig. 12).

Transcriptomic analysis revealed upregulation of genes associated with 'lymphocyte homing' and 'lymphoid follicle regulation' in EAEO cauda epididymidis (Suppl. Fig. 13A). Gene sets related to B- and T-cell activation were also enriched (Suppl. Fig. 13B, C). However, genes associated with complex function of TLO such as germinal centre activity were not found among the highly elevated DEGs. Consistent with bacterial epididymitis, B- and T-cell clusters were observed exclusively in the cauda epididymidis and not in other epididymal regions (Suppl. Fig. 13D). Finally, the lymphoid aggregates in EAEO cauda epididymidis were less developed compared to TLOs observed following UPEC infection. Given these findings, it can be speculated that the formation and maturation of TLO, in the cauda epididymidis, is dependent on the strength and type of inflammatory stimulus.

Patients with epididymitis show evidence of TLO formation in the cauda epididymidis

Having demonstrated that the murine cauda epididymidis is susceptible to TLO formation under inflammatory conditions, we extended these findings to the clinical setting. We analyzed specimens from three patients who underwent semicastration due to fulminant epididymitis with secondary testicular infarction, to detect key elements of TLO formation. The cauda epididymidis in these patients exhibited fibrotic remodeling and immune cell infiltration, similar to observations in our experimental animal models (Fig. 7A, E). Clusters of T-cells ($CD3^+$) and B-cells ($CD20^+$) were detected in various regions of the cauda epididymidis (Fig. 7B-C, F-G). Furthermore, HEVs ($MECA\text{-}79^+$) were identified within the immune cell clusters, providing evidence of cellular TLO elements in the cauda epididymidis of affected patients (Fig. 7D-H). Control human cauda epididymidis showed normal histology without pathological alterations (Fig. 7I, M). In contrast, in the normal epididymis, B-cells were very scarce, while T-cells were found more frequent and localized at the basal part of the epithelial layer beside the interstitial space (Fig. 7J-K, N-O). In a separate cohort of patients with acute epididymitis (n = 20), the majority of whom were infected with *E. coli*, serum levels of B-cell-attracting chemokine 1 (BCA-1, synonym CXCL13), were measured at presentation and during follow-up at 2 weeks and 3 months after antibiotic treatment. CXCL13 levels were significantly elevated in epididymitis patients compared to healthy controls (Fig. 8A). Following antibiotic treatment, CXCL13 levels decreased in most of the patients (Fig. 8B), however not reaching the healthy control levels. These findings provide evidence that TLO formation is also present in the human cauda epididymidis after inflammation (see Fig. 9).

Discussion

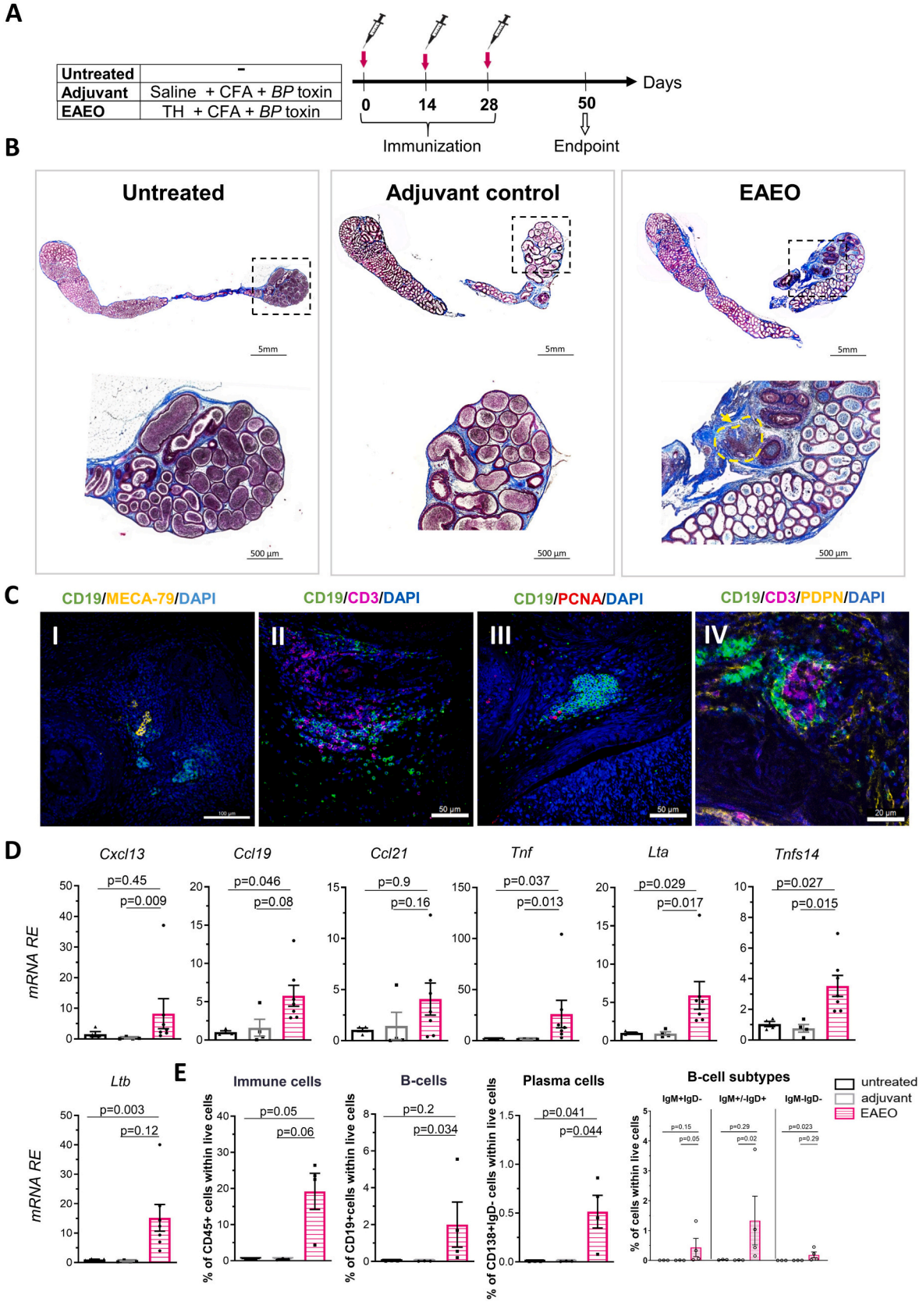
Despite successful antibiotic treatment and eradication of the pathogens ~ 40 % of epididymitis patients experience significantly reduced semen parameters.[2–4] Yet, the mechanisms leading to disturbances of fertility are poorly understood. Therefore, we aimed to investigate the immunopathological consequences of the bacterial infection on the cauda epididymidis during the post-acute and chronic phase of the disease. We demonstrate for the first time that UPEC infection leads to the formation of complex and mature tertiary lymphoid organs (TLO) in the murine cauda epididymidis. In this regard, TLOs were defined by the presence of organized clusters of B- and T-cells containing HEV and germinal centres (GC) resembling a lymph node in structure, especially during the chronic phase of the disease at 28 d.p.i. (Fig. 9). Moreover, in a translational part of our studies, we confirmed the findings from a preclinical mouse model and detected TLO elements also in patients suffering epididymitis.

The availability of murine tissues collected longitudinally at multiple time points from the UPEC infection model allowed us to investigate key factors involved in TLO formation, from the earliest time point of the infection until the chronic phase of the disease. B-cells were proliferative and expressed AID by 28 d.p.i., indicative of GC formation. We confirmed GC presence indirectly by detecting the capacity of the TLOs to activate the molecular machinery to sustain *in situ* differentiation of class-switched antibody-producing B-cells. Indeed, we detected the presence of IgG isotype-switched B-cells and plasma cells in UPEC-infected epididymidis. These findings are consistent with earlier studies reporting elevated concentrations of epididymal and systemic IgG and IgM antibodies during UPEC epididymitis in mice at 10 and 31 d.p.i..[54]

Although the presence of TLO has been reported in seminoma and testicular germ cell tumors,[27–29] we did not observe TLO formation in the UPEC infected testis at either 10 or 28 d.p.i. Consistent with previous findings, the testis exhibited immune cell infiltration and signs of spermatogenesis disruption during the acute phase of infection.[52] Despite a slight increased proportion of immune cells, including IgD^-IgM^- B-cells, at 28 d.p.i. spermatogenesis recovered. These findings collectively suggest that the inflammatory process in the testis is milder to that in the cauda epididymidis.

The presence of isotype switched antibodies produced by a local germinal centre in the epididymis is supported by the presence of a reticular network, which provides structural support and influences immune-cell migration and antibody formation.[45–46] Immune-cell separation into B- and T-cell zones at 28 d.p.i. was likely enabled by the high expression of mediators essential for ectopic lymphoid organogenesis following infection, including TLO-related chemokines *Ccl19, Ccl21* and *Cxcl13* (Fig. 8). These findings are consistent with the fact that inflammatory cytokines (TNF), TLO-related chemokines, and lymphotoxins (LTβ and LTα) are known to influence TLO formation, complexity and GC generation.[55–57] Results from our transcriptomic analysis of the murine infected cauda epididymidis confirmed the existence of an environment conducive for TLO induction, formation, and maintenance.

We also detected separate zones of B- and T-cells harboring HEV in epididymis sections from patients with chronic epididymitis, with B- and T-cell clusters and HEVs. Interestingly, some of the downregulated genes (e.g. *Cyp51, Gstm1, Mapk3a, Ptgs1, Trim2*) found in the murine UPEC-



(caption on next page)

Fig. 6. Tertiary lymphoid organ elements and lymphoid chemokines are present in the cauda epididymidis during EAEO. Timeline of EAEO induction and organ collection in C57BL6/J mice (A). Representative Azan-stained paraffin sections from untreated, adjuvant-control, and EAEO cauda epididymides, with an arrow indicating immune cell infiltrates (B). Immunofluorescence staining of CD19 (green) and MECA-79 (yellow) (I), CD3 (pink) and CD19 (green) (II), CD19 (green) and PCNA (red) (III), and CD19 (green), CD3 (pink) and PDPN (yellow) (IV) with DAPI-stained nuclei (blue) in EAEO cauda epididymides (C). Relative expression (RE) of *Cxcl13, Ccl19, Ccl21, Tnf, Lta, Tnfs14,* and *Ltb* mRNA in untreated, adjuvant, and EAEO cauda epididymides was measured by qRT-PCR and normalized to *Rplpo* (n = 4–7; mean ± SEM). Statistical analysis used Kruskal–Wallis test followed by Dunn's multiple comparison test, or one-way ANOVA followed by Tukey's multiple comparison test (D). Percentages of $CD45^+$ immune cells and $CD45^+CD19^+$ B-cells, $CD45^+CD19^-IgD^-CD138^+$ plasma cells, and isotype-switched B-cells ($CD45^+CD19^+IgM^+IgD^-$, $CD45^+CD19^+IgM^{+/-}IgD^-$, $CD45^+CD19^+IgM^-IgD^-$) in untreated, adjuvant, and EAEO cauda epididymides were determined by flow cytometry (n = 3–4; mean ± SEM). Statistical analysis used Kruskal–Wallis test followed by Dunn's multiple comparison test (E). (For interpretation of the references to colour in this figure legend, the reader is referred to the web version of this article.)

infected cauda epididymidis, are known to be involved in the impairment of male fertility.[58–62] In agreement with such impairment, we found elevated CXCL13 levels in the serum of affected patients during follow-up after acute epididymitis and despite adequate antibiotic treatment. This may account for B-cell recruitment into the epididymis and the formation of GCs producing antibodies. It is important to note that the elevated CXCL13 levels observed in epididymitis patients may indicate systemic inflammation or an inflammatory process in other organ. In this context, the measurement of CXCL13 directly in the seminal plasma would provide more specific insight into the local inflammatory environment. However, the collection of ejaculate during the acute phase of infection is contraindicated and thus present a significant limitation. Findings from a preclinical bacterial epididymitis mouse model showed that antiphlogistic treatment (dexamethasone) combined with antibiotic therapy (levofloxacin) dampens adaptive immunity by inducing a significant reduction in systemic IgG and IgM levels.[54] Data to support such a therapeutic regimen in humans are not available due to ethical and medical reasons. Taking diagnostic biopsies from the human epididymis for a comprehensive TLO analysis would cause irreversible iatrogenic obstruction. Such material is solely obtained following semicastration, a procedure that is rarely performed in fulminant epididymitis refractory to conservative treatment, i.e. when testicular involvement with secondary infarction occurs. Moreover, obtaining biopsies from epididymitis patients of bacterial origin is contraindicated as this would allow the bacteria to disseminate to other regions.[4]

The gradual increase in TLO complexity and structure that we observed following infection implies that TLOs are highly plastic and interchangeable, and depends on the local microenvironment and the strength of the inflammatory stimuli.[16] We were intrigued to note varying TLO complexity and morphology between our EAEO and UPEC infection models. In particular, we observed more advanced TLO structures in the cauda epididymidis in the UPEC model compared to the EAEO model. Such variability and plasticity has, however, been previously reported in other contexts. Recent data have shown that the murine cauda epididymidis, but not the proximal regions or testis develop early forms of TLO following the depletion of regulatory T-cells.[30] The study provides a comprehensive analysis of B- and T-cells diversity, immune mediators and antibody response associated with TLO formation in an epididymitis model induced by depletion of regulatory T cells. Furthermore, kidneys from aged mice contained early-stage TLOs, whereas kidneys from mice with polynephritis exhibited complex TLOs.[63] Moreover, poorly organized infiltrates that lack HEVs were observed in the pancreas of a spontaneous mouse model of type 1 diabetes at 8 weeks after induction, which gained a higher degree of organization, B- and T-cell compartmentalization and HEVs by 20 weeks.[64] To add, TLOs with no distinct B- or T-cell zones in kidneys from patients with mild pyelonephritis damage were detected, but TLOs with clearly separated B- and T-cells, an active GC, and follicular dendritic cells were present in highly destroyed areas.[63]

While the proximal regions are heavily populated with resident macrophages, the cauda is enriched in cells with innate-like characteristics (γδ T-cells, dendritic cells and natural killer cells) and different subclasses of dendritic cells that could influence TLO induction, maturation, and maintenance.[9,15] Furthermore, the macrophages present in the cauda epididymidis are more pro-inflammatory in function or display dendritic cell phenotypes that exhibit higher expression of phagosome-, antigen processing- and antigen presenting-related genes compared to other epididymal regions.[12–13] Consistently, at 10 d.p.i., an increase in the expression of genes that encode pro-inflammatory cytokines (e.g. *Il-1α, Il-6, Il-17*) and chemokines (e.g. *Ccl2, Ccl3, Cxcl13*) in the cauda epididymidis, but not in the caput, is reported. Previous transcriptomic analyses of the cauda epididymidis at 10 d.p.i. showed elevated expression of gene sets related to B- and T-cell activation.[9] Moreover, UPEC tends to persist in the cauda epididymidis longer and in higher numbers compared to other parts of the epididymis.[9] Considering that the cauda epididymidis harbors immunogenic spermatozoa, damage to the epithelial barrier could be sufficient impetus to promote a persistent adaptive immune response.[9] Altogether, these data provide a rational explanation for why the cauda develops TLO as a consequence of inflammation, while other parts of the epididymis do not.

Our findings provide a new molecular framework explaining the specific development of TLO in the cauda epididymidis as a consequence of inflammation. In conclusion, our data provide an account of TLO development in an organ harboring spermatozoa and open new avenues to the understanding how UPEC infection causes fertility damage in epididymitis patients. In addition to the epididymal damage observed in the cauda, the formation of lymphoid organ harboring an active germinal centre capable of locally producing antibodies possibly against spermatozoa also could contribute to fertility issues. Furthermore, investigations into the fertility-associated consequences of TLO formation in the cauda epididymidis are now warranted.

Data availability.

The data presented in this study are available in the article and supplementary material. Transcriptome data are available online at the GEO repository GSE282584 and GSE280507.

CRediT authorship contribution statement

Hiba Hasan: Writing – review & editing, Writing – original draft, Visualization, Validation, Methodology, Investigation, Formal analysis, Conceptualization. **Christiane Pleuger:** Writing – review & editing, Methodology, Investigation. **Dingding Ai:** Writing – review & editing, Investigation. **Sudhanshu Bhushan:** Writing – review & editing, Methodology, Investigation. **Eva Wahle:** Writing – review & editing, Investigation. **Tara Procida-Kowalski:** Writing – review & editing, Investigation, Formal analysis. **Qunxiong Zeng:** Writing – review & editing, Investigation. **Rukmali Wijayarathna:** Writing – review & editing, Resources, Investigation, Formal analysis. **Claire Xin Sun:** Writing – review & editing, Methodology, Investigation, Formal

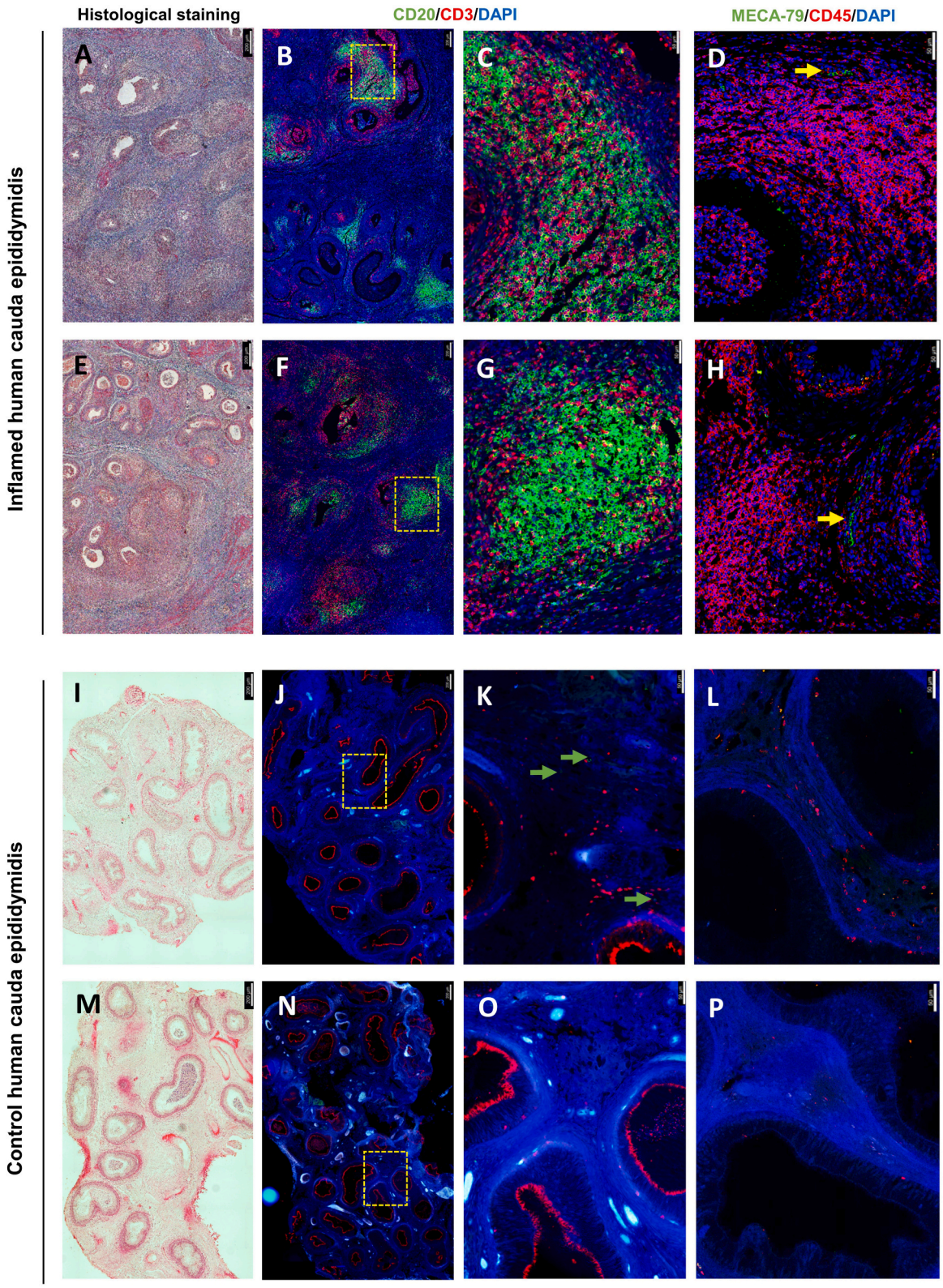


Fig. 7. Tertiary lymphoid organ elements are present in the epididymis of patients with chronic epididymitis. Representative Azan-stained paraffin sections of cauda epididymides from patients with a history of epididymitis (A, E) and H&E stained paraffin section of cauda epididymidis from patients serving as controls (I, M). Immunofluorescence staining for CD20 (green), CD3 (red) (B, C, F, G, J, K, N and O), and CD45 (red) with MECA-79 (green) (D, H, L and P), with DAPI (blue) staining for nuclei in cauda epididymides from epididymitis patients and control donors. Arrows in (D and H) indicate HEVs and B-cells in (K). Of note, in the images J, N, K and O autofluoroscence in the green channel and non-specific binding of CD3 in the stereocilia present in the apical part of the lumen of the epididymis are evident. (For interpretation of the references to colour in this figure legend, the reader is referred to the web version of this article.)

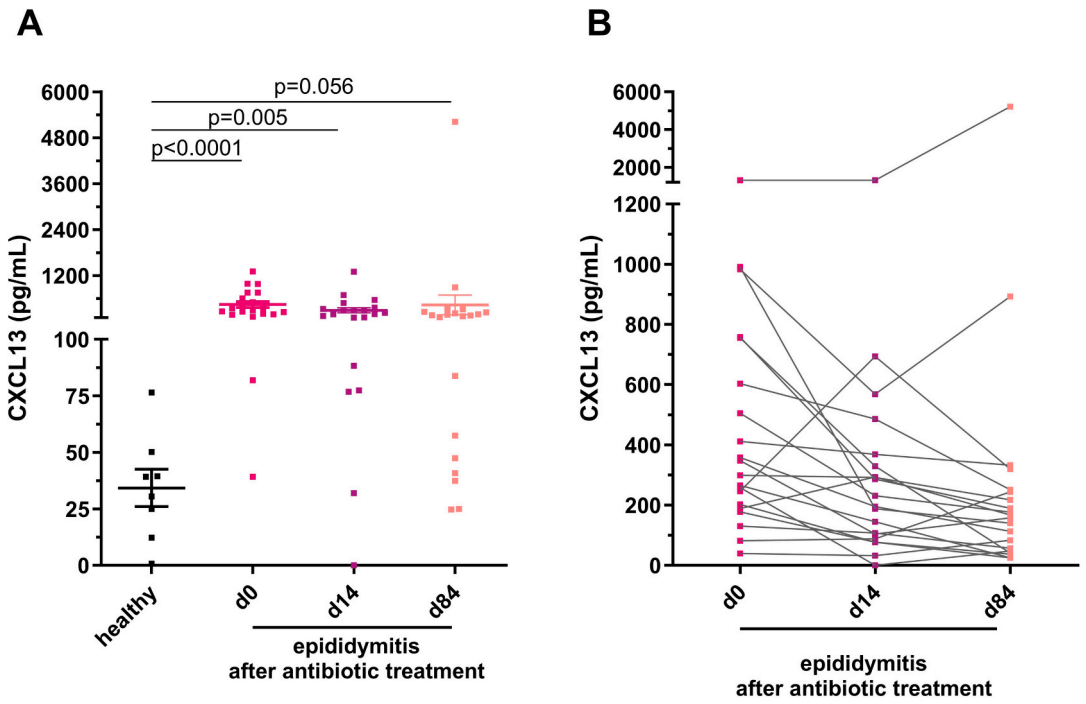


Fig. 8. Serum CXCL13 concentrations are elevated in patients with acute epididymitis. CXCL13 levels were analyzed in serum from healthy donors (n = 9) and epididymitis patients with (n = 10) or without abscess (n = 10) before and 2 weeks and 3 months post- antibiotic treatment using ELISA (A). CXCL13 levels were monitored by ELISA before, and at 2 weeks and 3 months following antibiotic treatment in the same patients across all three time points (B). Statistical analysis used the Kruskal–Wallis test.

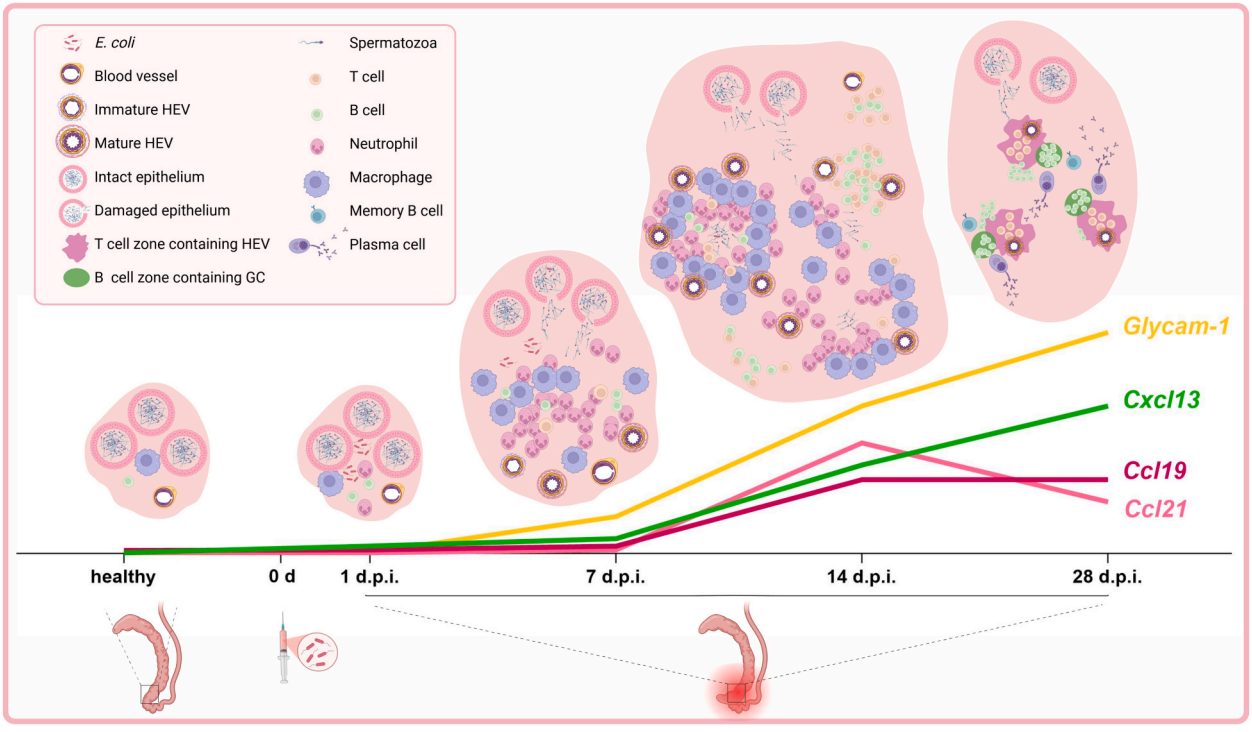


Fig. 9. UPEC infection leads to the formation of tertiary lymphoid organs (TLOs) in the mouse cauda epididymidis. At 1 day post-infection (d.p.i.), neutrophils and macrophages are recruited to the cauda epididymidis. By 7 d.p.i., GLYCAM-1 expression increases, along with markers associated with high endothelial venule (HEV) formation and subsequent maturation, enabling the development of HEVs. At this stage, HEVs recruit more immune cells compared to normal blood vessels. This process is accompanied by epithelial barrier destruction, where newly recruited immune cells target spermatozoa and bacteria. By 14 d.p.i., clear abscesses are observed. HEVs surrounding these abscesses are fully functional and capable of recruiting large numbers of immune cells. By 28 d.p.i., lymphoid chemokines, such as CXCL13, CCL19, and CCL21, increase, facilitating the recruitment of B- and T-cells. Some B- and T-cell clusters begin to compartmentalize into TLOs. Within these TLOs, B-cells, supported by T-cell zones containing HEVs, undergo germinal centre (GC) reactions. These reactions involve B-cell proliferation, affinity-based maturation, and differentiation into specialized B-cells, including memory B-cells and plasma cells, which produce high-affinity antibodies. Figure created with BioRender.

analysis. **Yong-Gang Duan:** Writing – review & editing, Resources, Investigation. **Daniela Fietz:** Writing – review & editing, Resources. **Marek Bartkuhn:** Writing – review & editing, Methodology, Investigation, Formal analysis. **Hans-Christian Schuppe:** Writing – review & editing, Resources, Investigation. **Adrian Pilatz:** Writing – review & editing, Resources, Investigation. **Kate L. Loveland:** Writing – review & editing, Funding acquisition, Formal analysis. **Andreas Meinhardt:** Writing – review & editing, Supervision, Funding acquisition, Formal analysis. **Mark P. Hedger:** Writing – review & editing, Supervision, Resources, Investigation, Funding acquisition, Formal analysis, Conceptualization. **Monika Fijak:** Writing – review & editing, Validation, Supervision, Resources, Project administration, Investigation, Funding acquisition, Formal analysis, Conceptualization.

Acknowledgments

This work was supported by the International Research Training Group in "Molecular pathogenesis on male reproductive disorders", a collaboration between Justus Liebig University (Giessen) and Monash University (Melbourne) (GRK1871/1-2) funded by the Deutsche Forschungsgemeinschaft and Monash University, a National Health and Medical Research Council of Australia Ideas Grant (1184867), and the Victorian Government's Operational Infrastructure Support Programme. This study was also supported by funding from the Deutsche Forschungsgemeinschaft (DFG, grant no. FI 1801/5-1 to M.F.).

Appendix A. Supplementary data

Supplementary data to this article can be found online at https://doi.org/10.1016/j.mucimm.2025.10.001.

References

1. Pilatz A, et al. Acute epididymitis revisited: impact of molecular diagnostics on etiology and contemporary guideline recommendations. *Eur Urol*. 2015;68:428–435.
2. Eickhoff JH, Frimodt-Møller N, Walter S, Frimodt-Møller C. A double-blind, randomized, controlled multicentre study to compare the efficacy of ciprofloxacin with pivampicillin as oral therapy for epididymitis in men over 40 years of age. *BJU Int*. 1999;84.
3. Rusz A, et al. Influence of urogenital infections and inflammation on semen quality and male fertility. *World J Urol*. 2012;30:23–30.
4. Fijak M, et al. Infectious, inflammatory and 'autoimmune' male factor infertility: how do rodent models inform clinical practice? *Hum Reprod Update*. 2018;24:416–441.
5. Pleuger C, Silva EJR, Pilatz A, Bhushan S, Meinhardt A. Differential immune response to infection and acute inflammation along the epididymis. *Front Immunol*. 2020;11:1–8.
6. De Grava Kempinas W, Klinefelter GR. Interpreting histopathology in the epididymis. *Spermatogenesis*. 2014;4.
7. Sullivan R, Mieusset R. The human epididymis: its function in sperm maturation. *Hum Reprod Update*. 2016;22.
8. Weigel Muñoz M, et al. Physiological and pathological aspects of epididymal sperm maturation. *Mol Aspects Med*. 2024;100.
9. Pleuger C, et al. The regional distribution of resident immune cells shapes distinct immunological environments along the murine epididymis. *Elife*. 2022;11.
10. Rinaldi VD, et al. An atlas of cell types in the mouse epididymis and vas deferens. *Elife*. 2020;9.
11. Battistone MA, et al. Immunoregulatory mechanisms between epithelial clear cells and mononuclear phagocytes in the epididymis. *Andrology*. 2024;12.
12. Battistone MA, et al. Region-specific transcriptomic and functional signatures of mononuclear phagocytes in the epididymis. *Mol Hum Reprod*. 2020;26.
13. Mendelsohn AC, et al. From initial segment to cauda: a regional characterization of mouse epididymal CD11c+ mononuclear phagocytes based on immune phenotype and function. *Am J Physiol Cell Physiol*. 2020;319:C997–C1010.
14. Voisin A, et al. Comprehensive overview of murine epididymal mononuclear phagocytes and lymphocytes: unexpected populations arise. *J Reprod Immunol*. 2018;126:11–17.
15. Ruddle NH. Basics of inducible lymphoid organs. *In Curr Top Microbiol Immunol*. 2020;426.
16. Sato Y, Silina K, van den Broek M, Hirahara K, Yanagita M. The roles of tertiary lymphoid structures in chronic diseases. *Nat Rev Nephrol*. 2023. https://doi.org/10.1038/s41581-023-00706-z.
17. Van De Pavert SA, Mebius RE. New insights into the development of lymphoid tissues. *Nat Rev Immunol*. 2010;10.
18. Drayton DL, Liao S, Mounzer RH, Ruddle NH. Lymphoid organ development: from ontogeny to neogenesis. *Nat Immunol*. 2006;7.
19. Neyt K, Perros F, GeurtsvanKessel CH, Hammad H, Lambrecht BN. Tertiary lymphoid organs in infection and autoimmunity. *Trends Immunol*. 2012;33:297–305.
20. Pipi, E. et al. Tertiary Lymphoid Structures : Autoimmunity Goes Local. **9**, 1–21 (2018).
21. Schumacher TN, Thommen DS. Tertiary lymphoid structures in cancer. *Science*. 1979;375:2022.
22. Blanchard, L. & Girard, J.P. High endothelial venules (HEVs) in immunity, inflammation and cancer. Angiogenesis (Springer Netherlands, 2021).doi:10.1007/s10456-021-09792-8.
23. Ruddle NH. High endothelial venules and lymphatic vessels in tertiary lymphoid organs: characteristics, functions, and regulation. *Front Immunol*. 2016;7.
24. Korpos É, et al. Identification and characterisation of tertiary lymphoid organs in human type 1 diabetes. *Diabetologia*. 2021;64.
25. Haidl G, Allam JP, Schuppe HC. Chronic epididymitis: Impact on semen parameters and therapeutic options. *In Andrologia*. 2008. https://doi.org/10.1111/j.1439-0272.2007.00819.x.
26. Schuppe H, Bergmann M. Atlas on the Human Testis. *Atlas on the Human Testis*. 2013;113–121. https://doi.org/10.1007/978-1-4471-2763-5.
27. Sakai Y, Hoshino H, Kitazawa R, Kobayashi M. High endothelial venule-like vessels and lymphocyte recruitment in testicular seminoma. *Andrology*. 2014;2.
28. Klein B, et al. Specific immune cell and cytokine characteristics of human testicular germ cell neoplasia. *Human Reproduction*. 2016;31:2192–2202.
29. Fietz D, Schuppe H-C, Loveland KL. Immunobiology of testicular. *Cancer.*. 2022 https://doi.org/10.1007/16833_2022_7.
30. Elizagaray ML et al. Chronic inflammation drives epididymal tertiary lymphoid structure formation and autoimmune fertility disorders. *bioRxiv* (2024).doi:10.1101/2024.11.12.623224.
31. Welch RA, et al. Extensive mosaic structure revealed by the complete genome sequence of uropathogenic Escherichia coli. *Proc Natl Acad Sci U S A*. 2002;99.
32. Peng W, et al. Activin A and CCR2 regulate macrophage function in testicular fibrosis caused by experimental autoimmune orchitis. *Cell Mol Life Sci*. 2022;79:602.
33. Nicolas N, et al. Testicular activin and follistatin levels are elevated during the course of experimental autoimmune epididymo-orchitis in mice. *Sci Rep*. 2017;7:1–15.
34. Kranz J, et al. European association of urology guidelines on urological infections: summary of the 2024 guidelines. *Eur Urol*. 2024;86:27–41.
35. Michel V, et al. Uropathogenic Escherichia coli causes fibrotic remodelling of the epididymis. *J Pathol*. 2016;240:15–24.
36. Kiernan, J. Histological And Histochemical Methods: Theory and Practice. In *Hodder Arnold Publications* **6th**, (2015).
37. Livak KJ, Schmittgen TD. Analysis of relative gene expression data using real-time quantitative PCR and the 2-ΔΔCT method. *Methods*. 2001;25:402–408.
38. Tommaso PD, et al. Nextflow enables reproducible computational workflows. *Nat Biotechnol*. 2017;35:316–319.
39. Love MI, Huber W, Anders S. Moderated estimation of fold change and dispersion for RNA-seq data with DESeq2. *Genome Biol*. 2014;15:550.
40. Blighe K, Rana S, Lewis M. EnhancedVolcano: Publication-ready volcano plots with enhanced colouring and labeling. R package version 1.24.0, https://github.com/kevinblighe/EnhancedVolcano. . (2024).
41. Gu Z, Eils R, Schlesner M. Complex heatmaps reveal patterns and correlations in multidimensional genomic data. *Bioinformatics*. 2016;32:2847–2849.
42. Xu S, et al. Using clusterProfiler to characterize multiomics data. *Nat Protoc*. 2024;19:3292–3320.
43. Tsyganov K, Perry A, Archer S, Powell D. MonashBioinformaticsPlatform/RNAsik-pipe: JOSS ready . (2018). doi:10.5281/zenodo.1403976.
44. Powell, D. drpowell/degust 4.1.1. (2019). doi:10.5281/zenodo.3501067.
45. Astarita JL, Acton SE, Turley SJ. Podoplanin: emerging functions in development, the immune system, and cancer. *Front Immunol*. 2012;3.
46. Cinti I, Denton AE. Lymphoid stromal cells—more than just a highway to humoral immunity. *Oxf Open Immunol*. 2021;2.
47. Klein U, Dalla-Favera R. Germinal centres: Role in B-cell physiology and malignancy. *Nat Rev Immunol*. 2008;8.
48. Shabgah AG, Shariati-Sarabi Z, Tavakkol-Afshari J, Mohammadi M. The role of BAFF and APRIL in rheumatoid arthritis. *J Cell Physiol*. 2019;234.
49. Gatto D, Brink R. The germinal center reaction. *J Allergy Clin Immunol*. 2010;126:898–907.
50. Srikakulapu P, et al. Artery tertiary lymphoid organs control multilayered territorialized atherosclerosis B-cell responses in Aged ApoE-/- mice. *Arterioscler Thromb Vasc Biol*. 2016;36:1174–1185.
51. Jones E, Gallimore A, Ager A. Defining high endothelial venules and tertiary lymphoid structures in cancer. *Methods Mol Biol*. 2018;1845:99–118.
52. Klein B, et al. Differential tissue-specific damage caused by bacterial epididymo-orchitis in the mouse. *Mol Hum Reprod*. 2020;26.
53. Wijayarathna R, et al. Region-specific immune responses to autoimmune epididymitis in the murine reproductive tract. *Cell Tissue Res*. 2020;381:351–360.
54. Klein B, et al. Dexamethasone improves therapeutic outcomes in a preclinical bacterial epididymitis mouse model. *Human Reproduction*. 2019;34:1195–1205.
55. Manzo A, et al. Systematic microanatomical analysis of CXCL13 and CCL21 in situ production and progressive lymphoid organization in rheumatoid synovitis. *Eur J Immunol*. 2005;35.
56. Thaunat O, et al. Lymphoid neogenesis in chronic rejection: evidence for a local humoral alloimmune response. *Proc Natl Acad Sci USA*. 2005;102.
57. Weyand CM, Goronzy JJ. Ectopic germinal center formation in rheumatoid synovitis. *In Ann N Y Acad Sci*. 2003;987.
58. Keber R, Rozman D, Horvat S. Sterols in spermatogenesis and sperm maturation. *J Lipid Res*. 2013;54.

59. Li JJ, et al. A recessive Trim2 mutation causes an axonal neuropathy in mice. *Neurobiol Dis*. 2020;140.
60. Pierucei-Alves F, Duncan CL, Schultz BD. Testosterone upregulates anion secretion across porcine vas deferens epithelia in vitro. *Biol Reprod*. 2009;81:628–635.
61. Ying HQ, Qi Y, Pu XY, Liu SR, Zhou-Cun A. Association of GSTM1 and GSTT1 genes with the susceptibility to male infertility: result from a meta-analysis. *Genet Test Mol Biomarkers*. 2013;17:535–542.
62. Li MWM, Mruk DD, Cheng CY. Mitogen-activated protein kinases in male reproductive function. *Trends Mol Med*. 2009;15:159–168.
63. Sato Y, et al. Developmental stages of tertiary lymphoid tissue reflect local injury and inflammation in mouse and human kidneys. *Kidney Int*. 2020;98:448–463.
64. Penaranda C, Tang Q, Ruddle NH, Bluestone JA. Prevention of diabetes by FTY720-mediated stabilization of peri-islet tertiary lymphoid organs. *Diabetes*. 2010;59.